Submitted to *PhysChemChemPhys*

Guided Ion Beam and Theoretical Studies of the Reaction of Ru^+ with CS_2 in the Gas-phase: Thermochemistry of RuC^+, RuS^+, and $RuCS^+$

P. B. Armentrout*

Department of Chemistry, University of Utah, 314 S. 1400 E. Rm 2020, Salt Lake City, Utah, 84112

Ilona Kretzschmar

Department of Chemical Engineering, The City College of New York, New York, NY 10031

Received ...

Abstract: The gas-phase reactivity of the atomic transition metal cation, Ru^+, with CS_2 is investigated using guided-ion beam mass spectrometry (GIBMS). Endothermic reactions forming RuC^+, RuS^+, and $RuCS^+$ are observed. Analysis of the kinetic energy dependence of the cross sections for formation of these three products yields the 0 K bond energies of $D_0(Ru^+\text{-}C)$ = 6.27 ± 0.15 eV, $D_0(Ru^+\text{-}S)$ = 3.04 ± 0.10 eV, and $D_0(Ru^+\text{-}CS)$ = 2.59 ± 0.18 eV, and consideration of previous data leads to a recommended $D_0(Ru^+\text{-}C)$ bond energy of 6.17 ± 0.07 eV. A detailed reaction coordinate surface for these processes is determined by quantum chemical calculations and shows that all three reactions take place by insertion to form a S-Ru^+-CS intermediate. Although multiple spin states are available, the reaction appears to occur primarily on the quartet ground state surface, although coupling to a sextet surface is required to form the $RuS^+(^6\Sigma^+)$ + $CS(^1\Sigma^+)$ ground state products. Calculations are used to locate the approximate crossing points between the quartet and sextet surfaces, finding them in both the bending coordinate of the S-Ru^+-CS intermediate and in the exit channel. Elimination of S_2 to form RuC^+ follows a much more complicated pathway involving a cyclic $RuCSS^+$ intermediate, consistent with the energetic behavior of the experimental RuC^+ cross section.

UU IR Author Manuscript

1. Introduction

Ruthenium sulfide is known to be one of the most active hydrotreating catalysts,[1] in particular in both unsupported and supported forms for hydrodesulfurization (HDS).[2,3] Adatoms such as zirconium or cesium appear to strengthen the Ru-S bond[4,5] in supported systems, thereby increasing the activity of the catalyst. In addition, nanosized ruthenium sulfide has been stabilized in yttrium zeolites and shows much higher activity than commercially available catalysts.[6-10] A density functional study of the low Miller index RuS_2 surfaces under hydrotreating conditions reveals a very high Lewis acidity of accessible metallic ruthenium surface sites.[11] These sites are likely to attract S-atoms, explaining the high HDS reactivity of RuS_2 nanoparticles. In a model system for these surface sites, RuS_2 nanoislands grown on a reconstructed Au (111) surface under ultra-high-vacuum conditions were found to exhibit sulfur vacancies in the RuS_2 (111) plane.[12] The catalytic activity of ruthenium sulfide towards hydrogen activation inspired the study of ruthenium sulfide loaded gas diffusion electrodes as working electrodes in fuel cells.[13] Although the activity for H_2 oxidation is lower on RuS_2 compared to Pt electrodes, RuS_2 electrodes are less sensitive to CO poisoning. In recent years, the synthesis of RuS_2 nanoparticles without support has been of interest because of their semiconducting properties. RuS_2 nanoparticles synthesized in a colloidal dimethylsulfoxide (DMSO) dispersion have a narrow size distribution, exhibit a strong fluorescence, and show strong interaction with dibenzothiophene and toluene.[14] Interestingly, thiol-capped monodisperse ruthenium nanoparticles also show evidence of Ru-S bonds and polycrystallinity.[15] Despite its importance in such catalytic applications, there are few studies of intrinsic structure and properties of small ruthenium sulfide complexes. Spectroscopic studies of RuS_2 molecules isolated in an argon matrix have been performed.[16] In addition, several Ru_xS_y metal organic complexes have been synthesized with Ru_2S_2[17] and Ru_4S_n cores (n = 4 - 6)[18] and it has been shown that the C-S bond of carbon disulfide is activated by ruthenium metal organic complexes.[19-22]

In previous work, we have investigated the gas-phase thermodynamic properties of the sulfides of first-row[23-31] and several early[31,32] and late[33-35] second-row transition metal cations, as

UU IR Author Manuscript

well as reviewed the periodic trends in this information.[36] In the present study, we investigate the gas-phase thermodynamic properties of the sulfide and thiocarbonyl of ruthenium. The reactions of the atomic cation of this element with carbon disulfide, CS_2, have previously been studied at room temperature in a high pressure of He by Bohme and coworkers,[37] who observed only $Ru^+(CS_2)$ adduct formation. In the present work, the reaction of Ru^+ with CS_2 is studied under single collision conditions using guided-ion beam mass spectrometric (GIBMS) techniques. The endothermic reactions 1 – 3 are observed and their dependence on kinetic energy is measured.

$$Ru^+ + CS_2 \rightarrow RuC^+ + S_2 \quad (1)$$

$$\rightarrow RuS^+ + CS \quad (2)$$

$$\rightarrow RuCS^+ + S \quad (3)$$

An analysis of the kinetic energy dependence permits the endothermicities of these reactions to be measured and converted to the 0 K bond dissociation energies, $D_0(Ru^+\text{-}C)$, $D_0(Ru^+\text{-}S)$, and $D_0(Ru^+\text{-}CS)$. Quantum-chemical methods are employed to complement the thermodynamic data with information on electronic ground and low-lying excited states, bond lengths, and vibrational frequencies of RuC^+, RuS^+, and $RuCS^+$. In addition, the reaction coordinate surfaces for the reactions are explored in order to ascertain the mechanisms with explicit consideration of spin-conservation requirements.

2. Methods

2.1. Experimental Section. GIBMS is used for the evaluation of thermodynamic data by means of threshold measurements of endothermic reactions. Detailed descriptions of the guided-ion beam apparatus used in this study and the experimental procedures are given elsewhere.[38,39] Briefly, Ar^+ ions created in a dc discharge source[39] are accelerated toward a ruthenium metal cathode thereby sputtering off Ru^+ ions. The metal ions drift in a meter-long flow tube operated with a 9:1 mixture of helium and argon at a pressure of ~90 Pa. The ions undergo ~10^5 collisions with the buffer gas before exiting the flow tube, and therefore are expected to equilibrate to room temperature. In previous work, comparison of a series of atomic metal cations produced using

the flow tube source and those created by surface ionization suggested that the temperature of the ions formed in the flow tube source is <1100 K.[40] This study and further studies of Ru^+ with O_2[41] and alkanes[42] found no evidence for excited states for Ru^+ ions formed in the flow tube, however, the present study shows evidence for electronically excited species, as discussed below. Because helium and argon need not effectively quench excited states of atomic transition-metal ions,[43,44] methane is introduced ca. 25 cm downstream from the discharge at pressures between 0.5 and 4.0 mTorr. Operation at these pressures allows the ions to undergo 10^2 - 10^3 collisions with these gases in the flow tube, which is sufficient to remove excited states of the Ru^+, as demonstrated below.

Following extraction from the source, the ions are accelerated and focused into a magnetic sector, mass-selected, decelerated to a desired kinetic energy, and focused into an octopole ion trap.[38,45] This device guides the ions through a static gas cell kept at a low pressure (~ 0.007 - 0.013 Pa) of the reactant gas. It was verified that all product cross sections reported result from single ion-molecule collisions by examining the pressure dependence of the product intensities. After exiting the gas cell, product and unreacted Ru^+ ions drift to the end of the octopole where they are directed into a quadrupole mass filter for mass analysis and then detected. Conversion of the raw ion intensities into reaction cross sections and the calibration of the absolute energy scale are treated as described previously.[38] The accuracy of the absolute cross sections is estimated to be ± 20 %. The beams have Gaussian kinetic energy distributions with average full widths at half maximum (FWHM) of ca. 0.25 eV in the laboratory frame. The uncertainty of the absolute energy scale is ± 0.05 eV (lab).

2.2. Data Analysis. Quantitative analysis of the energy dependence of these cross sections is achieved using eq 4 and methods outlined elsewhere.[46,47]

$$\sigma(E) = \sigma_0 \Sigma\, g_i\, (E + E_i - E_0)^n / E^m \qquad (4)$$

Here, E is the relative kinetic energy of the reactants, E_0 is the threshold for reaction at 0 K, σ_0 is an energy-independent scaling parameter, and n and m (usually set to unity) are fitting parameters describing the energy dependence. The summation is over the rovibrational states of the reactants

having energies E_i and populations g_i ($\Sigma g_i = 1$), with molecular parameters for CS_2 taken from B3LYP/Def2TZVPP calculations performed here (see below) for consistency. (Vibrational frequencies agree with experiment[48] within 3% and the rotational constants are the same.)

In addition to modeling the reaction product cross sections independently using eq 4, we also examine competition between the three reaction channels by using a statistical approach that has been described in detail elsewhere,[49,50] eq 5.

$$\sigma_j(E) = \left(n\sigma_{0,j}/E^m\right)\sum g_i \int_{E_{0,j}-E_i}^{E} \left[k_j(E^*)/k_{tot}(E^*)\right]\left[1-e^{k_{tot}(E^*)\tau}\right](E-\varepsilon)^{n-1}\,d(\varepsilon) \qquad (5)$$

Here $\sigma_{0,j}$ is a scaling parameter for channel j that is energy independent, $E_{0,j}$ represents the CID threshold energy for channel j at 0 K, ε is the energy available from reactant translation, and τ is the experimental time for dissociation (~100 μs in this instrument). E^* is the internal energy of the energized molecule (EM), i.e., $E^* = \varepsilon + E_i$. The term $k_j(E^*)$ is the unimolecular rate constant for dissociation of the EM to channel j. The rate constants $k_j(E^*)$ and $k_{tot}(E^*)$ are defined by Rice-Ramsperger-Kassel-Marcus (RRKM)[51-53] theory in eq 6,

$$k_{tot}(E^*) = \sum k_j(E^*) = \sum d_j N^{\dagger}_{j,vr}(E^* - E_{0,j})/h\rho_{vr}(E^*) \qquad (6)$$

where the sum is over all channels, d_j is the reaction degeneracy for channel j, h is Planck's constant, $N^{\dagger}_{j,vr}(E^* - E_{0,j})$ is the sum of rovibrational states of the transition state (TS) at an energy $E^* - E_{0,j}$ for channel j, and $\rho_{vr}(E^*)$ is the density of rovibrational states of the EM at the available energy, E^*. Transition states are treated as loose TSs at the phase space limit (PSL) for reactions 1 - 3,[49] with the additional possibility of a tight TS for reaction 1, as indicated theoretically (see below). Molecular parameters for the EM and TSs are taken from the quantum chemical calculations described below. In these models, the adiabatic 2-D rotational energy is treated using a statistical distribution with explicit summation over the possible values of the rotational quantum number, as described in detail elsewhere.[49]

Before comparison with the data, eqs 4 and 5 are convoluted over the translational energy distributions of both reactants. This determination of the reaction thresholds involves explicit consideration of the distributions of vibrational, rotational, and translational energies of both reactants. Because all sources of reactant energy are considered, the thermochemistry obtained

UU IR Author Manuscript

corresponds to 0 K values in all cases.

2.3. Theoretical Section. The bond lengths and the ground state/excited state splittings of RuC^+, RuS^+, and $RuCS^+$ are calculated at several levels of theory.

We perform calculations using the Gaussian 03 suite of programs[54] with the B3LYP hybrid density functional method[55,56] and Def2TZVPP basis sets, which are balanced basis sets of triple zeta valence quality, with contracted basis functions of [5s3p2d1f] for C, [5s5p3d1f] for S, and [6s4p3d2f1g] for Ru.[57,58] The Def2TZVPP basis set for Ru uses a small core (28 electron) effective core potential (ECP) developed by Andrae et al.[59] These basis sets were obtained from the EMSL basis set library.[60,61] In addition, to provide more accurate thermodynamic information, we also calculated single point energies of Ru^+, S, CS, CS_2, RuC^+, RuS^+, and $RuCS^+$ at the CCSD(T)/Def2TZVPP level of theory[62,63] using B3LYP/Def2TZVPP geometries and zero point energy corrections. This CCSD(T)/Def2TZVPP//B3LYP/Def2TZVPP level of theory was also used to examine the potential energy surfaces for the reactions. In all cases reported below, the single point energies cited include zero point energy corrections using unscaled B3LYP/Def2TZVPP vibrational frequencies. Finally, geometry optimizations at the CCD/Def2TZVPP (chosen because of the availability of analytic gradients) and CCSD(T) levels were performed on the ground states of RuC^+, RuS^+, and $RuCS^+$ to examine the dependence of the structures on the level of theory. Because the results presented below involve only the Def2TZVPP basis set, they will usually be distinguished only by the level of theory used.

The thermodynamic accuracy of these results can be assessed by comparing several well known quantities. At the CCSD(T) (B3LYP) levels of theory, C-S, S-CS, and S-S bond energies at 0 K are calculated to be 7.05 (7.14), 4.35 (4.70), and 4.08 (4.43) eV, respectively. These compare well with the experimental bond energies of 7.37 ± 0.04 eV,[64] 4.50 ± 0.04 eV,[64] and 4.364 ± 0.005 eV,[65] respectively, with a mean absolute deviation (MAD) of 0.25 ± 0.09 (0.17 ± 0.09) eV. Likewise, the average excitation energies of different spin states of Ru^+ are reproduced reasonably well. Experiment finds a $^4F(4d^7)$ ground state for Ru^+, with a $^6D(5s^14d^6)$ state at 1.09 eV and a $^2G(4d^7)$ state at 1.25 eV (average over all spin-orbit levels of all states).[66] Both levels of

UU IR Author Manuscript

theory reproduce the ^{4}F ground state and yield values of 0.62 (0.89) and 1.62 (1.53) eV, respectively, for the sextet and doublet excitation energies.

3. Theoretical Results

To fully understand the experimental results, it is important to know the nature of the electronic states of the RuC^+, RuS^+, and $RuCS^+$ species, as well as the pathways followed to form them. The calculations described above were used to provide this information. Relaxed potential energy scans, in which the likely reaction coordinate is systematically varied while all other coordinates are allowed to optimize, verify that all transition states connect the two adjacent intermediates.

3.1. RuC^+. B3LYP/Def2TZVPP calculations find a $^2\Delta$ ground state for RuC^+, Table 1. The ground state valence electron configuration is $(1\sigma)^2(1\pi)^4(2\sigma)^2(1\delta)^3(3\sigma)^0$ where the 1σ orbital is largely C(2s), the 2σ and 1π orbitals are the metal-carbon bonding orbitals, the 1δ are Ru(4d), the 3σ is largely Ru(5s), and 2π and 4σ are antibonding orbitals. Thus, this species has a triple bond with no antibonding orbitals occupied. Bond lengths calculated at the B3LYP and CCSD(T) levels of theory agree well with one another, whereas the CCD geometry optimization gives a bond length 0.09 Å shorter. Excitation from the 1δ to the 3σ orbital yields a $^4\Sigma^+$ state, lying 1.45 – 1.49 eV higher in energy. This excitation energy along with the much longer bond length, 1.669 Å versus 1.590 Å for the $^2\Delta$ ground state, indicate that the 3σ orbital has antibonding character. A $^2\Sigma^+$ state having the same electronic configuration (low-spin coupling of the 3σ with the 1δ orbitals) and a similar bond length as the $^4\Sigma^+$ state is found to lie 2.10 – 2.18 eV above the ground state. Still higher in energy are a $^4\Phi$ state, having a $(1\sigma)^2(1\pi)^3(2\sigma)^2(1\delta)^3(3\sigma)^1$ configuration, and a $^6\Pi$ state, with a $(1\sigma)^2(1\pi)^4(2\sigma)^1(1\delta)^2(3\sigma)^1(2\pi)^1$ configuration. The bond lengths for these states increase to 1.800 and 1.882 Å, respectively, consistent with the movement of bonding electrons into antibonding orbitals. Likewise, trends in the calculated vibrational frequencies match parallel expectations associated with the bond order of these states.

UU IR Author Manuscript

3.2. RuS^+. At the B3LYP/Def2TZVPP level of theory, calculations predict a $^6\Sigma^+$ ground state for RuS^+ with two close-lying quartet states ($^4\Phi/^4\Delta$) and two doublet states ($^2\Pi/^2\Sigma^+$), Table 1. The excitation energies of the quartet states range from 0.11 – 0.32 eV, whereas the doublet states range from 0.52 – 1.00 eV. The ground state valence electron configuration is $(1\sigma)^2(1\pi)^4(2\sigma)^2(1\delta)^2(3\sigma)^1(2\pi)^2$ where the 1σ orbital is largely S(3s), the 2σ and 1π orbitals are the metal-sulfur bonding orbitals, the 1δ are Ru(4d), the 3σ is largely Ru(5s), and 2π and 4σ are antibonding orbitals. This state can be viewed as donation of the doubly occupied 3p orbital of S into the empty 5s orbital of $Ru^+(^4F,4d^7)$ with the three electron holes in the $4d_\sigma$ and both $4d_\delta$ orbitals. The quartet states have configurations of $(1\sigma)^2(2\sigma)^2(1\pi)^4(1\delta)^3(3\sigma)^1(2\pi)^1$ and $(1\sigma)^2(1\pi)^4(2\sigma)^2(1\delta)^3(3\sigma)^0(2\pi)^2$, respectively. The doublet states have $(1\sigma)^2(1\pi)^4(2\sigma)^2(1\delta)^4(3\sigma)^0(2\pi)^1$ and $(1\sigma)^2(1\pi)^4(2\sigma)^2(1\delta)^4(3\sigma)^1(2\pi)^0$ configurations, respectively. Not surprisingly, given the populations of the antibonding 2π orbitals, the bond lengths decrease and the vibrational frequencies increase from the sextet to the quartet to the doublet states, Table 1. Geometries of the ground state determined at three different levels of theory agree reasonably well with one another, with the CCSD(T) bond length lying between the B3LYP and CCD results, Table 1.

3.3. $RuCS^+$. The ground state of ruthenium thiocarbonyl is calculated to be a $^4\Sigma^+$ state corresponding to binding of CS to the ^4F ground state of Ru^+. As shown in Table 2, the CS bond length in this molecule is slightly shorter than in free CS by 0.015 – 0.039 Å. Consistent with this, the vibrational frequency of the CS bond stretch increases from 1311 cm^{-1} to 1417 cm^{-1}. Geometries calculated at the B3LYP, CCD, and CCSD(T) levels of theory agree reasonably well, with the CCSD(T) and B3LYP agreeing very closely. The $^4\Sigma^+$ state has a valence electron configuration of $(1\sigma)^2(2\sigma)^2(1\pi)^4(3\sigma)^2(2\pi)^4(1\delta)^2(4\sigma)^1$, where the 1σ, 2σ, and 1π orbitals are the carbon-sulfur bonding orbitals, the 3σ is a metal-carbon bond formed by donation of the HOMO of CS into a 5s-4d hybrid on Ru, the 2π are the backbonding interactions between the metal and the antibonding π orbitals on CS, the 1δ are Ru(4d), the 4σ is the other Ru(5s-4d) hybrid, and the 3π and 5σ are Ru-C antibonding orbitals. Similar results are also found for a low-lying doublet

UU IR Author Manuscript

$^2\Delta$ state, which lies 0.39 – 0.54 eV higher in energy but has a much shorter Ru-C bond length, 1.794 versus 1.878 Å. Here, the electron configuration is $(1\sigma)^2(2\sigma)^2(1\pi)^4(3\sigma)^2(2\pi)^4(1\delta)^3(4\sigma)^0$. In contrast, a $^6A''$ state has a bent geometry with a much longer Ru-C bond length (2.101 Å) and a lower CS bond stretch (1214 cm^{-1}). Using linear symmetry designations, this state has a $(1\sigma)^2(2\sigma)^2(1\pi)^4(3\sigma)^2(2\pi)^3(1\delta)^2(4\sigma)^1(3\pi)^1$ configuration in which one of the backbonding 2π orbitals is singly occupied, which explains why the molecule is bent. The sextet species lies quite high in energy, 2.41 - 2.54 eV above the $^4\Sigma^+$ ground state, such that it is bound by only 1.28 (1.63) eV relative to the $Ru^+(^6D)$ + CS asymptote at the CCSD(T) (B3LYP) levels of theory. In contrast, the ground state is bound by 3.28, 3.06, and 3.02 eV at the B3LYP, CCSD(T)/B3LYP, and CCSD(T)/CCD levels of theory.

3.4. Potential Energy Surfaces – Bond Insertion. The reaction coordinate diagram for reaction of CS_2 with Ru^+ in the quartet, sextet, and doublet spin states is shown in Figure 1. The energies used in this diagram were calculated at the CCSD(T)//B3LYP level of theory and these values will be used throughout the following discussion. Geometries for the reactants, intermediates, and products are shown in Figures 2 – 4 for the quartet, doublet, and sextet spin states, respectively, in the same order as one moves across Figure 1, with energies and structural parameters provided in Table 3. All of the species are planar with the exception of several of the sextet states, as indicated in Figure 4 by specifying the ∠SRuCS dihedral angle.

The initial interaction of Ru^+ and CS_2 forms Ru^+(SCS) complexes, Figure 1a, where the metal ion is bound to the carbon for all three spin states, Figures 2 – 4. Geometry optimizations started with linear RuSCS structures always collapsed to bent geometries or converged to species with imaginary bending frequencies. For the quartet and doublet states, the Ru^+(SCS) complexes have C_{2v} symmetry with the CS bond lengths slightly extended from free CS_2 and with the CS_2 bond angle between 171 – 179°, Table 3. The overall ground state is the $^4B_1$ state, with $^2A_1$, $^2A_2$, $^2A_1$, and $^2B_2$ states lying 0.46, 0.69, 0.73, and 1.58 eV, respectively, higher in energy. The $^4B_1$ state is bound by 1.93 eV relative to the $Ru^+(^4F)$ + CS_2 reactants, whereas the $^2A_1$ state is bound by 3.09 eV relative to the $Ru^+(^2G)$ + CS_2 asymptote. This is consistent with the shorter Ru-C

UU IR Author Manuscript

bond length and the larger perturbation of the CS_2 ligand in the doublet states (except the $^2B_2$). The $^6A'_a$ state of Ru^+(SCS) lies 2.00 eV above the $^4B_1$ state and is much more weakly bound, 0.55 eV relative to the $Ru^+(^6D)$ + CS_2 asymptote because of the repulsive interaction of the closed shell CS_2 with the occupied 5s orbital on Ru^+. This molecule has one of the few nonplanar geometries among the species calculated here, with a ∠SRuCS dihedral angle of 145° and a much more strongly distorted ∠SCS bond angle of 136°. A sextet state having a planar geometry ($^6A'_b$) was located in which the Ru^+ ion sits over one of the CS bonds, thereby lengthening this bond and distorting the ∠SCS bond angle to 133°. This state lies 0.66 eV above the $^6A'_a$ nonplanar structure. Additional planar sextet states were located (both A′ and A″ symmetries) but had imaginary frequencies corresponding to out-of-plane bends and were higher in energy by 0.33 and 0.46 eV, respectively, at the B3LYP/Def2TZVPP level of theory.

Along the quartet surface, reaction takes place by oxidative addition of a CS bond to the ruthenium center, leading to the transition state TS($^4A''$) followed by the SRu^+(CS) ($^4A''$) intermediate, Figure 2. The $^4A''$ intermediate can be viewed as donation of the σ(CS) lone pair of electrons (the HOMO) into the empty 3σ orbital of RuS^+ ($^4\Delta$). The bent geometry permits a backbonding interaction from a 1δ orbital of RuS^+ to CS, stabilizing the bent configuration compared to a linear geometry. As the ∠SRuC bond angle is increased from the $^4A''$ intermediate, the energy rises monotonically (as shown in Figure 1 and discussed in detail below), such that the lowest energy linear form of the quartet SRu^+(CS) intermediate (a $^4\Phi$ state located 1.34 eV above the $^4A''$ state, Table 3) collapses to the bent form (imaginary frequency of 126 cm^{-1}). However, at slightly higher energies, 1.71 eV above the $^4A''$ state, a stable $^4\Delta$ state is found. This state has longer RuS and RuC bonds than the $^4A''$ state, and very low degenerate bending frequencies of 93 cm^{-1}.

We also explored whether an equivalent pathway exists having $^4A'$ symmetry, but find that it is much higher in energy. The Ru^+(SCS) intermediate located has $^4B_2$ symmetry but an imaginary frequency of 79 cm^{-1} that corresponds to an out-of-plane bend. Thus, this species will collapse to the much lower $^4B_1$ ground state. The SRu^+(CS) ($^4A'$) intermediate and its

UU IR Author Manuscript

corresponding bond insertion TS were found to be stable, but quite high in energy, 1.37 and 2.37 eV, respectively, higher than their $^4A''$ counterparts. In essence, these species correspond to the low-spin equivalents of the sextet species discussed below, but are higher in energy in accordance with Hund's rules.

Along the doublet surface, the reaction proceeds in a parallel fashion to the quartet surface, Figure 1. Surfaces of both $^2A''$ and $^2A'$ symmetry were located and are very similar in energy. Oxidative addition of a CS bond to the ruthenium center leads to transition states TS($^2A''$) and TS($^2A'$), which have similar geometries to TS($^4A''$), Figures 2 and 3. The imaginary frequencies of 312 and 357 cm^{-1}, respectively, again correspond to the expected CS stretching motion. These transition states go on to form $SRu^+(CS)$ intermediates having the appropriate symmetry. The intermediates have slightly longer RuS bonds compared to the $^2\Pi$ state of the RuS^+ product and slightly longer RuC bonds compared to the $^2\Delta$ state of the $Ru^+(CS)$ product, Figure 4. Similar to the quartet state, these intermediates can be viewed as donation of the σ(CS) lone pair of electrons into the empty 3σ orbital of RuS^+ ($^2\Pi$), with the occupation of the 2π orbitals determining A′ versus A″ symmetry. Again the bent geometry is favored because this allows back-donation from the 1δ orbital of RuS^+ to the CS π^* orbitals. As the ∠SRuC bond angle increases, the energy increases eventually forming a linear $^2\Delta$ state of $SRu^+(CS)$, 1.43 eV above the $^2A''$ bent intermediate. The linear state has two imaginary frequencies corresponding to bending motions in both planes, and thus will collapse to the bent geometries, Figure 1a.

The sextet surface is distinct from the lower spin surfaces, Figure 1a. As noted above, the initial interaction between $Ru^+(^6D)$ and CS_2 is much less attractive. The energy required to move from $Ru^+(SCS)$ (^6A) to the insertion TS is 0.56 eV, comparable to the barrier height for the quartet and doublet states (0.61 - 0.63 eV). The ^6A transition state is close to being planar with a ∠SRuCS dihedral angle of 179°. The RuS and RuC bond lengths in the sextet TS are much longer than those in the quartet and doublet states, Figure 4. Furthermore, the sextet state of the $SRu^+(CS)$ intermediate is now linear, $^6\Sigma^+$, with RuS and RuC bond lengths longer than the lower spin counterparts, Figure 4. Examination of the potential energy surface from the TS to the

UU IR Author Manuscript

$SRu^+(CS)$ linear intermediate shows that the energy decreases monotonically (as detailed below), although there is an inflection point near ∠SRuC = 120°. Importantly, the sextet state is the lowest energy linear intermediate, such that the sextet surface must cross those of the quartet and doublet spins along this bending coordinate, Figure 1a, as discussed in more detail below.

3.5. Potential Energy Surfaces – Product Formation. As shown in Figure 1b, from the bent $SRu^+(CS)$ ($^4A''$) intermediate, cleavage of the metal ligand bonds can lead to both RuS^+ + CS and $Ru^+(CS)$ + S product channels. If spin is conserved, the accessible product channel for reaction 2 is RuS^+ ($^4\Pi$) + CS ($^1\Sigma^+$), which is an excited state for this channel, Table 1. For reaction 3, the situation is more complex because of the triplet spin of the sulfur atom product. Adiabatically, the $SRu^+(CS)$ ($^4A''$) ground state intermediate correlates with the $Ru^+(CS)$ ($^4\Sigma^+$) + S (^3P) ground state products, however, formation of $Ru^+(CS)$ ($^2\Delta$) + S (^3P) and $Ru^+(CS)$ ($^6A''$) + S (^3P) is also spin conserving.

Likewise, the $^2A''$ and $^2A'$ states of the bent $SRu^+(CS)$ intermediate lead to RuS^+ ($^2\Delta$) + CS ($^1\Sigma^+$), which is an excited state for this channel, if spin is conserved. As for the quartet intermediate, the $^2A''$ and $^2A'$ states of the $SRu^+(CS)$ intermediate adiabatically correlate with the ground state $Ru^+(CS)$ ($^4\Sigma^+$) + S (^3P) asymptote, but spin is also conserved to form $Ru^+(CS)$ ($^2\Delta$) + S (^3P). Finally, from the $SRu^+(CS)$ ($^6\Sigma^+$) intermediate, the ground state products of reaction 2, RuS^+ ($^6\Sigma^+$) + CS ($^1\Sigma^+$), can be formed in a spin-conserving process. Adiabatically, this intermediate again correlates with the ground state $Ru^+(CS)$ ($^4\Sigma^+$) + S (^3P) asymptote, but spin is also conserved to form $Ru^+(CS)$ ($^6A''$) + S (^3P).

We also considered whether the initially formed $Ru^+(SCS)$ intermediates might decompose directly to RuS^+ + CS; however, because of the proximity of the metal cation to the CS bond in these intermediates, cleavage of the S-CS bond leads to the bond insertion intermediates along all three spin surfaces.

Formation of the minor RuC^+ + S_2 products in reaction 1 is more complicated than the simple bond fission processes of reactions 2 and 3, but formation of the $SRu^+(CS)$ intermediates is again involved, Figure 1b. From these intermediates, coupling of the two sulfurs leads to

UU IR Author Manuscript

cyclic transition states (TS_{SS}) as shown in Figures 2 – 4. Because of the cyclic structure, these transition states have fairly similar geometries, with RuS bond lengths increasing to 2.14 – 2.26 Å, CS bonds increasing to 1.58 – 1.69 Å, and RuC bonds remaining nearly constant as the S-S distances decrease to 2.21 – 2.75 Å. The quartet and doublet transition states are planar, but the sextet state is nonplanar with an ∠SRuCS dihedral angle of 31°. For the quartet and doublet surfaces, these transition states lie 1.52 – 1.62 eV above the $SRu^+(CS)$ bent intermediates, whereas TS_{SS} (^6A) lies 2.60 eV above the linear $^6\Sigma^+$ intermediate. From these transition states, cyclic c-$RuCSS^+$ intermediates are formed and have similar energies (Figure 1b) and geometries (Figures 2 – 4) as their respective transition states. Again these species are planar except for the sextet state. A planar form of the sextet intermediate was located but has an imaginary frequency of 97 cm^{-1} that is an out-of-plane bend.

Formation of the $RuC^+ + S_2$ products can occur from the cyclic intermediates by cleaving the RuS and CS bonds, which occurs stepwise. If the CS bond cleaves first, the system passes over TS_{CS} on its way to forming $CRu^+(SS)$ intermediates, Figure 1b. The imaginary frequencies correspond to CS stretches where the CS bond has increased by 0.40 – 0.74 Å compared to the c-$RuCSS^+$ intermediates, and concomitantly, the S-S bond shortens by 0.08 – 0.17 Å. The TS_{CS} transition states lie 0.14 ($^2A'$) to 0.80 ($^4A''$) eV above the c-$RuCSS^+$ intermediates and 0.14 ($^2A'$) to 0.58 ($^4A''$) eV above the $CRu^+(SS)$ intermediates having the same spin. The $^2A''$ TS_{CS} has an additional imaginary frequency of 10 cm^{-1} that is an out-of-plane bend, such that this species collapses to the lower energy $^2A'$ surface. The doublet and sextet states of the $CRu^+(SS)$ intermediates have open planar structures, Figures 3 and 4, with short RuC (1.60 – 1.70 Å), short S-S (1.88 – 1.96 Å), and long RuS (2.21 – 2.49 Å) bond lengths. A $^4A''$ state having a similar structure was located but has an imaginary out-of-plane bend (14 cm^{-1}) that allows it to collapse to the nonplanar structure shown in Figure 2. The $^4A'$ state has a distorted tetrahedral geometry with the symmetry plane passing through the RuC bond and the center of the S-S bond. The lowest energy $^2A''_a$ state located contained an imaginary frequency (37 cm^{-1}, out-of-plane bend) that allows it to collapse to the $^2A'$ state, whereas a stable $^2A''_b$ state was found 0.17 eV higher in

UU IR Author Manuscript

energy. A nearly planar (∠SRuCS = 0.6°) ^{2}A state for CRu^+(SS) was also located only 0.16 eV above the ^{2}A′ state.

If the RuS bond cleaves first, the reaction proceeds via TS_{RuS} and formation of $RuCSS^+$ intermediates. The potential energy surface for the RuS bond cleavage pathway is shown in Figure S1 of the supporting information because it generally lies above the pathway where the CS bond is cleaved first. The imaginary frequencies of TS_{RuS} correspond to RuS stretches leading to long RuS bonds, 3.16 – 3.30 Å for the quartet and doublet states, which are considerably longer than that for the sextet state (2.54 Å). RuC and CS bond lengths are all about 1.7 – 1.8 Å. The lower spin TSs are planar, whereas the sextet TS_{RuS} is nonplanar with a ∠SRuCS dihedral angle of 17°. The doublet and quartet TS_{RuS} species lie 0.25 – 0.34 eV above the respective TS_{CS} species, but in contrast, $^6TS_{RuS}$ lies below $^6TS_{CS}$ by 0.23 eV. The $RuCSS^+$ intermediates all have similar planar geometries with nearly linear RuCS moieties and ∠CSS bond angles of 100 - 110°. All bond lengths are slightly extended from any of the products. The lower-spin intermediates lie 0.42 - 0.71 eV above the respective CRu^+(SS) intermediates, but again the sextet state lies 0.38 eV below its counterpart. Clearly, coupling of $S_2(^3\Sigma^+)$ to the ruthenium end of the RuC^+ molecule favors formation of covalent bonds and the low-spin states because the half-filled orbitals of RuC^+ are localized on the ruthenium center. If there is no covalent coupling between RuC^+ and S_2, as must be the case for the sextet states, interaction of S_2 at the carbon center is now favored.

From the CRu^+(SS) intermediates, products of reaction 1 are formed by simple cleavage of the RuS bond and by cleaving the CS bond from $RuCSS^+$ intermediates. Ground state $RuC^+(^2\Delta)$ + S_2 $(^3\Sigma^-)$ products can be formed from both the quartet and doublet intermediates, Figure 1b, whereas the sextet intermediate adiabatically dissociates to form the $RuC^+(^4\Sigma^+)$ + S_2 $(^3\Sigma^-)$ excited state asymptote, 1.45 eV higher in energy, Table 1. Binding energies for S_2 to the ruthenium end of RuC^+ are 1.63, 1.27, and 1.01 eV for the quartet, doublet, and sextet states, respectively, whereas binding S_2 to the carbon end yields binding energies of 0.92, 0.83, and 1.38 eV, respectively.

3.6. Quartet/Sextet Surface Crossings. The results above indicate that formation of

UU IR Author Manuscript

ground state RuS^+ ($^6\Sigma^+$) + CS ($^1\Sigma^+$) products from Ru^+ (^4F) + CS_2 ($^1\Sigma_g^+$) reactants in reaction 2 must involve coupling between the quartet and sextet surfaces. Coupling to the doublet surfaces might also occur but is not intrinsic to the observed reactivity and therefore was not explored. Clearly, spin-orbit coupling (enhanced by the presence of both the heavy metal and sulfur) as well as the character of the seam over which the spin surfaces interact will influence the efficiency of the spin change. To approximate the character of the crossing seam, we take the approach of Yoshizawa et al.[67] Thus, a relaxed potential energy surface scan conducted at the B3LYP/Def2TZVPP level along a likely region of coordinate space for each spin state is conducted and then single point energies of the other spin state at the same geometries are also calculated. As noted above, the regions where surfaces are likely to cross occur in both the region involving the SRuC bond angle (Figure 1a) as well as the dissociation coordinate (Figure 1b), i.e., stretching the SRu^+-CS bond.

Figure 5 shows the results of the relaxed potential energy surface scan calculations along with the geometries of the approximate crossing points (CPs). Their energies and geometric parameters are listed in Table 3. For the bending coordinate along the optimized quartet surface, Figure 5a, the crossing point (^{4}CP1) occurs near the linear form of the SRu^+(CS) intermediates, at a ∠SRuC bond angle of ~163°, r(Ru-C) = 2.14 Å, and an energy of -0.64 eV, Table 3. Along the sextet surface (Figure 5b), ^{6}CP1 again lies near the linear forms of the SRu^+(CS) intermediate at a bond angle of ~156°, r(Ru-C) = 2.12 Å, and an energy of -0.79 eV, Table 3. Because the well associated with the SRu^+(CS) intermediate lies considerably below the energies of the reactants and products, Figure 1, the lifetime of this species is likely to be sufficient to allow multiple passes through the crossing seam.

When the reaction coordinate for SRu^+-CS bond dissociation is examined, we find that the linear intermediates do not cross at all (not shown in Figure 5), consistent with the fact that the linear sextet intermediate and the sextet product asymptote are both lower in energy than the quartet surface. For dissociation from the bent quartet intermediate (Figure 5c), ^{4}CP2 lies at r(Rh-C) = 3.26 Å, ∠SRhC ~ 155°, and an energy of 0.41 eV, Table 3. Here, the surfaces lie close

UU IR Author Manuscript

and parallel to one another for an extensive distance, such that coupling again might be anticipated to be relatively efficient, although multiple passes through the ^{4}CP2 crossing point seem unlikely.

4. Experimental Results

4.1. Experimental Observations. Ru^+ reacts with CS_2 to yield three major products, RuC^+, RuS^+, and $RuCS^+$, formed in reactions 1 - 3, respectively. Unlike the flow tube studies of Bohme and coworkers,[37] no $Ru^+(CS_2)$ adducts are observed because the single collision conditions used here do not allow the collisional relaxation necessary to form such adducts. Product cross sections are depicted in Figure 6 for conditions where the reactant ions are either not cooled or cooled by collisions with methane in the flow tube ion source. Minor products observed are RuS_2^+ and CS_2^+ with cross sections below 0.06×10^{-16} cm^2 (not shown). Figure 6 shows that all three products exhibit small exothermic reaction cross sections followed by larger endothermic processes as the collision energy is increased. When methane is admitted to the flow tube source, the exothermic cross sections disappear, demonstrating that they are the result of electronically excited states of Ru^+. The energy dependence of the low energy feature is consistent with the Langevin-Gioumousis-Stevenson (LGS) collision cross section for ion-molecule reactions,[68] $\sigma_{LGS}(E) = (\pi q/4\pi\varepsilon_0)(2\alpha/E)^{1/2}$, where q is the charge on the ion, ε_0 is the permittivity of vacuum, E is the collision energy, and α is the polarizability of CS_2, 8.74 Å^3.[69] The magnitude of the total experimental cross section is about 0.2% of the LGS prediction, indicating that only a small percentage of excited states need be present to account for the observed reactivity. According to the thermochemistry derived below, neither the $Ru^+(^6D)$ nor the $Ru^+(^2G)$ states have sufficient energy to react exothermically with CS_2 in reactions 2 and 3, indicating that higher lying states must be responsible for the observed reactivity.

Product cross sections for Ru^+ ions formed with methane in the flow tube are shown in Figure 7, and should correspond to the reactivity of ground state $Ru^+(^4F)$. Formation of RuC^+ has the lowest energy threshold, near 1 eV. At slightly higher energies, the RuS^+ cross section rises

UU IR Author Manuscript

rapidly, far exceeding the magnitude of the thermodynamically favored RuC^+ product ion. Formation of $RuCS^+$ does not begin until about 1.8 eV with a cross section that rises much more slowly than the other two product ions.

At elevated collision energies, the RuS^+ and $RuCS^+$ cross sections can decline more rapidly because these products can dissociate in the overall process 7, starting at $D_0(SC\text{-}S) = 4.50 \pm 0.04$ eV.

$$Ru^+ + CS_2 \rightarrow Ru^+ + CS + S \qquad (7)$$

Although the $RuCS^+$ and total cross sections reach a maximum in good accord with this prediction, the cross section for RuS^+ peaks near 2.5 eV, which is well before 4.50 eV. One possible reason for the early peak in this cross section is competition with the $RuCS^+$ channel, which has a magnitude sufficient to account for the decline as demonstrated by the observation that the total cross section levels off but does not begin to decline until 4.5 eV. Likewise, dissociation of the RuC^+ product cannot occur until 7.50 ± 0.01 eV = $D_0(CS_2 \rightarrow C + S_2)$.[64,65] The early maximum near 2 eV found in this product cross section could be explained by competition with the formation of RuS^+. Indeed, the relative behavior in these two cross sections indicates that although $RuC^+ + S_2$ is thermodynamically favored, formation of $RuS^+ + CS$ must occur over a much looser transition state as it dominates the products shortly after its threshold. The possibility of such competition in both cases is assessed further below in the analysis of the data.

Another potential reason for the early decline in these cross sections is that they are spin-forbidden. In a detailed study of the reaction of V^+ with CS_2,[70] it was found that the cross-section for the VS^+ product formed in the analogue of reaction 2 also reaches a peak at low energies (below 4.5 eV). It was shown that this result could be quantitatively modeled by consideration of the energy dependence of the surface-crossing probability for a spin-forbidden reaction. Briefly, higher energy reactants pass through the surface crossing region more rapidly, reducing the ability of the electrons to adjust to different configurations along the reaction coordinate, such that spin-forbidden paths become less efficient with higher energy. The probability of making the surface crossing has been shown to vary as the inverse of the velocity of the reactants through the

UU IR Author Manuscript

crossing region, essentially as $E^{-1/2}$. In our modeling, this can be introduced by utilizing a value for the parameter *m* of 1.5 in eqs 4 and 5, instead of the usual value of 1.0.[70] As noted above, the reaction of ground state Ru^+ (^4F) with CS_2 ($^1\Sigma^+$)[71] to form ground state RuS^+ ($^6\Sigma^+$) + CS ($^1\Sigma^+$) is spin-forbidden, however, formation of the ground state products $RuCS^+$ ($^4\Sigma^-$) + S (^3P) and RuC^+ ($^2\Delta$) + S_2 ($^3\Sigma^-$) are spin-allowed. Therefore, the early peak in the RuS^+ cross section, but not that of the RuC^+ cross section, could be attributed to the spin-forbidden character of the reaction.

4.2. Data Analysis. Careful analysis of the threshold regions for the cross sections of reactions 1 – 3 yields the σ_0, *n*, and E_0 values summarized in Table 4 for $m = 1.0$. Analysis was performed by analyzing the reaction channels independently using eq 4, in which case the values of *n* used to reproduce the data are distinct, ~0.8, ~1.1, and ~2.0 for reactions 1 - 3, respectively. This result properly reflects the very different rates at which the RuC^+ and RuS^+ versus $RuCS^+$ cross sections rise from threshold.

When these channels are analyzed as competitive reactions assuming loose PSL transition states for all three products, eq 5 is able to reproduce the data nicely throughout the threshold region, up to 4.5 eV, where reaction 7 can begin. In the competitive analysis, the value of *n* used is the same for all three channels. Similarly good reproduction is obtained for both $m = 1.0$ and 1.5 with nearly identical parameters except for *n*, which increases by about 0.5 in going from $m = 1.0$ to 1.5. The competitive analysis successfully reproduces the shape of the RuS^+ cross section, specifically the maximum at about 2.5 eV, demonstrating that this behavior can be attributed to competition with formation of $RuCS^+$. Likewise the early maximum in the RuC^+ cross section is reproduced well, demonstrating that this behavior is a result of competition with the formation of the favored RuS^+ product. Indeed, given that the threshold for RuC^+ is clearly lower than that for RuS^+, the relative behavior here demonstrates that formation of RuC^+ is much more constrained than that of the higher energy product. This finding is consistent with the reaction coordinate surfaces shown in Figure 1b. These surfaces suggest that the competition between the RuS^+ and $RuCS^+$ channels, which involve loose TSs, and the RuC^+ channel is influenced by the tight TSs on the way to the energetically limiting loose TS at the $RuC^+ + S_2$ product asymptote. Therefore,

UU IR Author Manuscript

the data were also modeled assuming a transition state switching model[72-74] in which the $RuC^+ + S_2$ channel was restricted by whichever TS, either the loose PSL TS or the tight TS_{CS} with molecular parameters and relative energy (0.25 ± 0.30 eV, Table 3) established by the calculations, has the lowest number of states at any particular energy of the EM. The optimized parameters of eq 5 from this model are also shown in Table 4 and Figure 8 shows the reproduction of the data. The fidelity of the fit is comparable to that for the model where all TSs are assumed to be loose.

The competitive analyses show that the main reason for the predominance of the $RuS^+ +$ CS channel compared to $RuCS^+ + S$ is the difference in the number of states available. Note the $RuS^+ +$ CS channel has 4 rotational and 2 vibrational degrees of freedom whereas the $RuCS^+ + S$ channel has 2 rotations and 4 vibrations. Indeed, if the competition between the two channels is calculated purely on the basis of the internal degrees of freedom, the $RuCS^+ + S$ channel would be even smaller. To reproduce the data, the $RuCS^+ + S$ channel needs to be increased by a factor of 10.2 ± 5.2 (loose TSs) or 10.3 ± 5.5 (switching TS) relative to the RuS^+ product channel, when the latter is assumed to have molecular parameters associated with the $^6\Sigma^+$ ground state. These scaling factors are represented by the different σ_0 values in Table 4. Note that the electronic degeneracy of the RuS^+ ($^6\Sigma^+$) + CS ($^1\Sigma^+$) channel is lower than that for the Ru^+(CS) ($^4\Sigma^-$) + S (^{3}P) channel, 6 versus 36, a factor of 6, which rationalizes the scaling factor needed. The fact that the latter channel can be formed with no spin change may also enhance its probability compared with the spin-forbidden formation of RuS^+. In this regard, we also analyzed the data assuming that the spin-allowed RuS^+ ($^4\Phi$) product is formed instead, where the ratio of electronic degeneracies for reactions 2 and 3 is now 8 versus 36, or a factor of 4.5. In this model, all the fitting parameters of eq 5 remain virtually identical, consistent with the small differences in the molecular parameters of these two states, Table 1.

A scaling factor for formation of RuC^+ relative to the RuS^+ ($^6\Sigma^+$) channel is also utilized in the fits shown in Figure 8. Here the scaling factors are 0.4 ± 0.1 (loose TSs) or 0.7 ± 0.6 (switching TSs), when the CS_2 and S_2 species are properly assigned rotational symmetries of 2.

UU IR Author Manuscript

The electronic degeneracy for formation of RuC^+ ($^2\Delta$) + S_2 ($^3\Sigma^-$) is 12 relative to 6 for RuS^+ ($^6\Sigma^+$) + CS ($^1\Sigma^+$), predicting a scaling factor of 2, in better agreement with the switching TS model. We note that the scaling factor in the switching TS model is quite sensitive to the energy of the tight TS, rising to 1.6 when this energy is assumed to be 0.55 eV (relative to reactants) and decreasing to 0.4 at a TS energy of -0.05 eV. This dependence accounts for the much larger uncertainty in the scaling factor and suggests that the energy of the tight TS could be somewhat higher than theoretically predicted or that TS_{SS} also decreases the probability of this pathway.

Finally, we note that the value of n used in these competitive fits is about 0.5 when m = 1.0 and loose transition states are assumed, which is much smaller than often encountered for reactions of this type. When m = 1.5, it rises to a more conventional value close to unity. When the transition state switching model is used, the n value rises to 0.7 ± 0.3 when m = 1.0 (1.2 for m = 1.5). This variation in the value of n is another indication that the tight transition state along the $RuC^+ + S_2$ reaction path definitely influences the competition among these channels.

The E_0 values of Table 4 can be converted to the Ru^+-C, Ru^+-S, or Ru^+-CS bond strengths at 0 K using eq 8 and D_0(SC-S) = 4.50 ± 0.04 eV or D_0(C-S_2) = 7.50 ± 0.01 eV, where X can represent either C, S, or CS.

$$D_0(Ru^+\text{-}X) = D_0(CS_2 - X) - E_0 \qquad (8)$$

The resultant bond energies are provided in Table 4. It can be seen that the values obtained from the competitive modeling are within experimental uncertainty of the independent analyses, where preliminary versions of the latter have been reported previously.[36] We believe that the more sophisticated competitive modeling, which reproduces all three cross sections simultaneously, provides the most accurate threshold values in addition to being more precise. There are some indications that the TS switching model that includes the tight TS for reaction 1 is more realistic, although both competitive models yield comparable threshold energies for all three channels. Overall, we recommend as our final values the average of the two competitive models (all loose TSs and switching TS): $D_0(Ru^+\text{-}C)$ = 6.27 ± 0.15 eV, $D_0(Ru^+\text{-}S)$ = 3.04 ± 0.10 eV, and $D_0(Ru^+\text{-}CS)$ = 2.59 ± 0.18 eV, where the uncertainties are two standard deviations.

UU IR Author Manuscript

5. Discussion

5.1. Thermochemistry. The calculated bond energy of the RuS^+ ground state is 3.13 eV at the B3LYP level of theory, 2.93 eV at the CCSD(T)//B3LYP and CCSD(T)//CCD, and 2.96 eV at the CCSD(T) levels of theory after basis set superposition error corrections in the full counterpoise limit[75,76] are applied, Table 5. These values are in good agreement with the experimental bond energy of 3.04 ± 0.10 eV. Because of spin-conservation (see further discussion below), it is possible that the experimental threshold corresponds to formation of the RuS^+ ($^4\Phi$) excited state. This species has calculated bond energies of 2.93 eV (B3LYP) and 2.69 eV (CCSD(T)/B3LYP), such that the more reliable CCSD(T) value disagrees with experiment. We conclude that the experiment produces ground state RuS^+ in a spin-forbidden process, a conclusion in concert with our previous results for the analogous reactions of CS_2 with Rh^+, Pd^+, and Ag^+.[33-35]

For the ruthenium thiocarbonyl cation, the theoretical ground state bond energies are 3.08, 2.94, 2.90, and 2.85 eV at the B3LYP, CCSD(T)/B3LYP, CCSD(T)/CCD, and CCSD(T) levels of theory, respectively, including counterpoise corrections, Table 5. These values are somewhat above the experimental value of 2.59 ± 0.18 eV, but with discrepancies comparable to those of the calibration calculations. For the $RuCS^+$ product, there are no spin restrictions in the formation of any states. Note that theory indicates that the Ru^+-S bond is stronger than the Ru^+-CS bond by only 0.00 – 0.11 eV (Table 5), whereas experiment finds differences of 0.37 – 0.47 eV, Table 5. Certainly the general appearance of the data, Figures 6 – 8, are not consistent with similar bond energies for these two species. It seems likely that because the metal-ligand bonding in these two molecules is distinct, covalent for RuS^+ and dative for $RuCS^+$, theory may not provide balanced views of both interactions.

The calculated bond energies for RuC^+ are 5.93, 5.94, 5.64, and 6.00 eV at the B3LYP, CCSD(T)/B3LYP, CCSD(T)/CCD, CCSD(T) levels of theory, respectively, including counterpoise corrections, Table 5. All these values are somewhat low compared to the

experimental value of 6.27 ± 0.15 eV, but the discrepancies with all but the CCD value are comparable to those of the calibration calculations. As there are no spin restrictions in the formation of the $RuC^+(^2\Delta)$ + $S_2(^3\Sigma^-)$ products, the formation of ground state products is anticipated. The only alternative neutral products that could be formed are RuC^+ + 2 S, but this leads to a bond energy for RuC^+ of 10.64 ± 0.10 eV, much too high to be reasonable.

The present experimental bond energy for the ruthenium carbide cation is well above that reported previously, 4.70 ± 0.11 eV.[77] This value was obtained by measuring the thresholds for formation of RuC^+ from reactions of $Ru^+(^4F)$ with ethane and cyclopropane. In the latter system, the observed threshold of 1.14 ± 0.04 eV was assigned to the formation of RuC^+ + C_2H_6. If this process actually corresponds to formation of RuC^+ + H_2 + C_2H_4, then the RuC^+ bond energy derived is 6.13 ± 0.04 eV, in good agreement with the present result. In this same system, a secondary threshold of 2.67 ± 0.12 eV was assigned to formation of RuC^+ + H_2 + C_2H_4, whereas if this corresponds to production of RuC^+ + 2 H_2 + C_2H_2, then the RuC^+ bond energy derived becomes 6.34 ± 0.12 eV, again in good agreement with the present result. For the ethane system, the threshold was assigned to formation of RuC^+ + H_2 + CH_4 because any other neutral products are too high in energy to be feasible. In this case, the process rises slowly from threshold and is probably hindered by competition with other reactions such that the measured threshold is likely to be an upper limit to the true thermochemistry. Further evidence for the accuracy of the RuC^+ bond energy obtained here comes from the qualitative observations in the reactions of Ru^+ with propane and iso-butane.[77] In these systems, formation of RuC^+ + 2 H_2 + C_2H_4 from propane and RuC^+ + 2 H_2 + C_3H_6 from isobutene are predicted to have thresholds of about 2.6 eV using $D_0(RuC^+)$ = 6.27 eV. In both cases, these predictions are in good agreement with the apparent thresholds observed. Overall, we believe the best experimental value for the RuC^+ bond energy is the weighted average of the present value and those obtained from the cyclopropane reaction, 6.16 ± 0.07 eV. This value is in reasonable agreement with those calculated at the B3LYP and CCSD(T)/B3LYP levels of theory.

It should be noted that the spin-orbit interactions in these three product ions may differ

UU IR Author Manuscript

appreciably. Experimental bond energies refer to the ground spin-orbit state at 0.0 eV, $^4F_{9/2}$ for Ru^+. In contrast, calculations are referenced to the statistically weighted mean of all spin-orbit levels in the ground state term, 0.175 eV for Ru^+ (^4F).[66] Because our calculations do not explicitly include spin-orbit interactions, it is possible that calculated bond energies should be reduced by this different asymptotic energy before comparison with experimental values. However, spin-orbit effects influence the energetics of all reactants, intermediates, and products with unknown and varying magnitudes. For instance, recent spectroscopic studies of RhS($^4\Sigma^-$) find a small spin-orbit splitting of 47.43 cm^{-1} (0.0059 eV) between the Ω = 3/2 and 1/2 states.[78] Given the uncertainties, we do not apply corrections in the present work, which implicitly assumes that the spin-orbit corrections largely cancel, which appears to be true for RuS^+, but not the other two product ions.

5.2. Reaction Mechanism. The reaction coordinate diagram of Figure 1 shows clearly that reactions 2 and 3 occur by insertion of the ruthenium cation into a CS bond of CS_2 followed by simple cleavage of one of the metal ligand bonds. The experimental results correspond to reaction of ground state Ru^+(^4F), which the calculations indicate can form the ground state Ru^+(CS) ($^4\Sigma^+$) + S (^3P) products by remaining on the quartet surface throughout the reaction. In contrast, formation of the ground state RuS^+ ($^6\Sigma^+$) + CS ($^1\Sigma^+$) products clearly requires a change in spin. Calculations indicate that crossing points between these surfaces lie well below the energy of the reactants in the region associated with the bending motion of the SRu^+(CS) intermediate, as well as along the dissociation coordinate, Figure 5. Because of the lifetime of the intermediate and the parallel nature of the two surfaces for dissociation, it is reasonable to expect that the coupling between spin surfaces is fairly efficient for this heavy metal system. This conclusion is consistent with the conclusions drawn from a comparison of the experimental and theoretical bond energies for the RuS^+ product.

Formation of the thermodynamically preferred RuC^+ + S_2 products in reaction 1 is also spin-allowed, but clearly entropically disfavored once the RuS^+ + CS products are accessible. Considering that reaction 1 requires cleavage of two bonds in the reactants and formation of two

UU IR Author Manuscript

new bonds (compared to one bond cleaved and one formed for reactions 2 and 3), it is not surprising that this process is more complicated and therefore disfavored. Calculations elucidate a detailed mechanism evolving again from the $SRu^+(CS)$ intermediates, followed by formation of constrained cyclic c-$RuCSS^+$ intermediates, which can then dissociate by sequential cleavage of RuS and CS bonds. The pathway involving CS bond cleavage to form $CRu^+(SS)$ intermediates followed by RuS bond cleavage to yield products is found to lie slightly lower in energy than the alternative pathway involving initial RuS bond cleavage to form open $RuCSS^+$ intermediates followed by CS bond cleavage to form products. Both pathways can probably contribute to the observed reactivity.

Acknowledgement

Profs. D. Schröder and H. Schwarz are thanked for their support and guidance when these data were taken. This work was supported by the Fonds der Chemischen Industrie (graduate fellowship for IK) and the National Science Foundation (PBA, CHE-0748790). In addition, we thank the Center for High Performance Computing at the University of Utah for the generous allocation of computer time.

References

(1) Pecoraro, T. A.; Chianelli, R. R. *J. Catal.* **1981**, *67*, 430.

(2) Castillo-Villalón, P.; Ramírez, J.; Louis, C.; Massiani, P. *Applied Catalysis A* **2008**, *343*, 1.

(3) De Los Reyes, J. A. *Applied Catalysis A* **2007**, *322*, 106.

(4) Eliche-Quesada, D.; Rodríguez-Castellón, E.; Jiménez-López, A. *Micropor. Mesopor. Mat.* **2007**, *99*, 268.

(5) Ishihara, A.; Lee, J.; Dumeignil, F.; Yamaguchi, M.; Hirao, S.; Qian, E. W.; Kabe, T. *J. Catal.* **2004**, *224*, 243.

UU IR Author Manuscript

(6) Moraweck, B.; Bergeret, G.; Cattenot, M.; Kougionas, V.; Geantet, C.; Portefaix, J. L.; Zotin, J. L.; Breysse, M. J. Catal. **1997**, *165*, 45.

(7) Blanchard, J.; Bando, K. K.; Matsui, T.; Harada, M.; Breysse, M.; Yoshimura Y. *Applied Catalysis A* **2007**, *322*, 98.

(8) Sun, C.; Peltre, M.-J.; Briend, M.; Blanchard, J.; Fajerwerg, K.; Krafft, J.-M.; Breysse, M.; Cattenot, M.; Lacroix, M. *Applied Catalysis A* **2003**, *245*, 245.

(9) Kougionas, V.; Cattenot, M.; Zotin, J. L.; Portefaix, J. L.; Breysse, M. *Appl. Catal. A* **1995**, *124*, 153.

(10) Dumonteil, C.; Lacroix, M.; Geantet, C.; Jobic, H.; Breyssey, M. *J. Catal.* **1999**, *187*, *464*.

(11) Aray, Y.; Vidal, A. B.; Rodriguez, J.; Grillo, M. E.; Vega, D.; Coll, D. S. *J. Phys. Chem. C* **2009**, *113*, 19545.

(12) Cai, T.; Song, Z.; Rodriguez, J. A.; Hrbek, J. *J. Am. Chem. Soc.* **2004**, *126*, 8886.

(13) Zhang, H.; Verde-Gomez, Y.; Jacobson, A. J.; Ramirez, A.; Chianelli, R. R. **2002**, *Mat. Res. Soc. Symp. Proc.* Vol 756, FF5.7,1.

(14) Díaz, D., Castillo-Blum, S. E.; Álvarez-Fregoso, O;. Rodríguez-Gattorno, G.; Santiago-Jacinto, P.; Rendon, L.; Ortiz-Frade, L.; León-Paredes, Y.-J. *J. Phys. Chem. B* **2005**, *109,* 22715.

(15) Chakroune, N.; Viau, G.; Ammar, S.; Poul, L.; Veautier, D.; Chehimi, M. M.; Mangeney, C.; Villain, F.; Fiévet, F. *Langmuir* **2005,** *21,* 6788.

(16) Liang, B.; Wang, X.; Andrews, L. *J. Phys. Chem. A* **2009**, *113,* 5375.

(17) Rauchfuss, T.B.; Rodgers, D. P. S.; Wilson, S. R. *J. Am. Chem. Soc.* **1986**, *108*, 3114.

(18) Eckermann, A. L.; Wunder, M.; Fenske, D., Rauchfuss, T. B.; Wilson, S. R. *Inorg. Chem.* **2002**, *41*, 2004.

(19) Pandey, K. K.; Tewari, S. K. *Polyhedron* **1989**, *8*, 1149.

(20) Planas, J. G.; Marumo, T.; Ichikawa, Y.; Hirano, M.; Komiya, S. *J. Mol. Catal. A* **1999**, *147*, 137.

UU IR Author Manuscript

(21) Padney, K. K. *Coord. Chem. Rev.* **1995**, *140*, 37.

(22) Petz, W. *Coord. Chem. Rev.* **2008**, *252*, 1689.

(23) Kretzschmar, I.; Schröder, D.; Schwarz, H.; Rue, C.; Armentrout, P. B. *J. Phys. Chem. A* **1998**, *102*, 10060-10073.

(24) Rue, C.; Armentrout, P. B.; Kretzschmar, I.; Schröder, D.; Harvey, J. N.; Schwarz, H. *J. Chem. Phys.* **1999**, *110*, 7858-7870.

(25) Schröder, D.; Kretzschmar, I.; Schwarz, H.; Rue, C.; Armentrout, P. B. *Inorg. Chem.* **1999**, *38*, 3474-3480.

(26) Bärsch, S.; Kretzschmar, I.; Schröder, D.; Schwarz, H.; Armentrout, P. B. *J. Phys. Chem. A* **1999**, *103*, 5925-5934.

(27) Kretzschmar, I.; Schröder, D.; Schwarz, H.; Rue, C.; Armentrout, P. B. *J. Phys. Chem. A* **2000**, *104*, 5046-5058.

(28) Kretzschmar, I.; Schröder, D.; Schwarz, H. *J. Phys. Chem. A* **2001**, *105*, 8456-8464.

(29) Rue, C.; Armentrout, P. B.; Kretzschmar, I.; Schröder, D.; Schwarz, H. *Int. J. Mass Spectrom.* **2001**, *210/211*, 283-301.

(30) Rue, C.; Armentrout, P. B.; Kretzschmar, I.; Schröder, D.; Schwarz, H. *J. Phys. Chem. A* **2002**, *106*, 9788-9797.

(31) Kretzschmar, I.; Schröder, D.; Schwarz, H.; Armentrout, P. B. *Int. J. Mass Spectrom.* **2003**, *228*, 439-456.

(32) Kretzschmar, I.; Schröder, D.; Schwarz, H.; Armentrout, P. B. *Int. J. Mass Spectrom.* **2006**, *249–250*, 263–278.

(33) Armentrout, P. B.; Kretzschmar, I. *J. Phys. Chem. A* **2009,** *113,* 10955–10965.

(34) Armentrout, P. B.; Kretzschmar, I. *Inorg. Chem.* **2009**, *48*, 10371–10382.

(35) Armentrout, P. B.; Kretzschmar, I. *J. Chem. Phys.* In press.

UU IR Author Manuscript

(36) Kretzschmar, I.; Schröder, D.; Schwarz, H.; Armentrout, P. B. *Advances in Metal and Semiconductor Clusters*, Duncan, M. A. (Ed.); **2001**, *5*, 347-394.

(37) Cheng, P.; Koyanagi, G. K.; Bohme, D. K. *J. Phys. Chem. A* **2006,** *110,* 2718-2728.

(38) Ervin, K. M.; Armentrout, P. B. *J. Chem. Phys.* **1985**, *83*, 166.

(39) Schultz, R. H.; Armentrout, P. B. *Int. J. Mass Spectrom. Ion Processes* **1991**, *107*, 29.

(40) Chen, Y.-M.; Elkind, J. L.; Armentrout, P. B. *J. Phys. Chem.* **1995**, *99*, 10438-10445.

(41) Chen, Y.-M.; Armentrout, P. B. *J. Chem. Phys.* **1995**, *103*, 618-625.

(42) Armentrout, P. B.; Chen, Y.-M. *J. Am. Soc. Mass Spectrom.* **1999**, *10*, 821-839.

(43) Kemper, P. R.; Bowers, M. T. *J. Phys. Chem.* **1991**, *95*, 5134.

(44) Haynes, C. L.; Armentrout, P. B. *Organometallics* **1994**, *13*, 3480.

(45) Gerlich, D. *Adv. Chem. Phys.* **1992**, *82 (Part 1)*, 1-176.

(46) Schultz, R. H.; Crellin, K. C.; Armentrout, P. B. *J. Am. Chem. Soc.* **1991**, *113*, 8590.

(47) Armentrout, P. B. in *Advances in Gas Phase Ion Chemistry*, Adams, N. G.; Babock, L. M., Eds.; JAI Press, Greenwich, **1992**, *1*, 83-119.

(48) Herzberg, G. *Molecular Spectra and Molecular Structure*; Van Nostrand Reinhold: New York, 1966; Vol. III.

(49) Rodgers, M. T.; Ervin, K. M.; Armentrout, P. B. *J. Chem. Phys.* **1997**, *106*, 4499.

(50) Rodgers, M. T.; Armentrout, P. B. *J. Chem. Phys.* **1998**, *109*, 1787.

(51) Gilbert, R. G.; Smith, S. C. *Theory of Unimolecular and Recombination Reactions*; Blackwell Scientific: London, **1990**.

(52) Truhlar, D. G.; Garrett, B. C.; Klippenstein, S. J. *J. Phys. Chem.* **1996**, *100*, 12771.

(53) Holbrook, K. A.; Pilling, M. J.; Robertson, S. H. *Unimolecular Reactions*, 2nd ed.; Wiley: New York, **1996**.

(54) Frisch, M. J.; Trucks, G. W.; Schlegel, H. B.; Scuseria, G. E.; Robb, M. A.; Cheeseman, J. R.; Montgomery, J., J. A. ; Vreven, T.; Kudin, K. N.; Burant, J. C.; Millam, J. M.; Iyengar, S. S.;

UU IR Author Manuscript

Tomasi, J.; Barone, V.; Mennucci, B.; Cossi, M.; Scalmani, G.; Rega, N.; Petersson, G. A.; Nakatsuji, H.; Hada, M.; Ehara, M.; Toyota, K.; Fukuda, R.; Hasegawa, J.; Ishida, M.; Nakajima, T.; Honda, Y.; Kitao, O.; Nakai, H.; Klene, M.; Li, X.; Knox, J. E.; Hratchian, H. P.; Cross, J. B.; Adamo, C.; Jaramillo, J.; Gomperts, R.; Stratmann, R. E.; Yazyev, O.; Austin, A. J.; Cammi, R.; Pomelli, C.; Ochterski, J. W.; Ayala, P. Y.; Morokuma, K.; Voth, G. A.; Salvador, P.; Dannenberg, J. J.; Zakrzewski, V. G.; Dapprich, S.; Daniels, A. D.; Strain, M. C.; Farkas, O.; Malick, D. K.; Rabuck, A. D.; Raghavachari, K.; Foresman, J. B.; Ortiz, J. V.; Cui, Q.; Baboul, A. G.; Clifford, S.; Cioslowski, J.; Stefanov, B. B.; Liu, G.; Liashenko, A.; Piskorz, P.; Komaromi, I.; Martin, R. L.; Fox, D. J.; Keith, T.; Al-Laham, M. A.; Peng, C. Y.; Nanayakkara, A.; Challacombe, M.; Gill, P. M. W.; Johnson, B.; Chen, W.; Wong, M. W.; Gonzalez, C.; Pople, J. A., Gaussian 03, Revision B.02, Revision B.02, 2003, Gaussian, Inc., Pittsburgh, PA.

(55) Becke, A. D. *J. Chem. Phys.* **1993**, *98*, 5648-5652.

(56) Lee, C.; Yang, W.; Parr, R. G. *Phys. Rev. B* **1988**, *37*, 785-789.

(57) Eichkorn, K.; Weigend, F.; Treutler, O.; Ahlrichs, R. *Theor. Chem. Acc.* **1997**, *97*, 119.

(58) Weigend, F.; Ahlrichs, R. *Phys. Chem. Chem. Phys.* **2005**, *7*, 3297.

(59) Andrae, D.; Haeussermann, U.; Dolg, M.; Stoll, H.; Preuss, H. *Theor. Chim. Acta* **1990**, *77*, 123-141.

(60) Feller, D. *J. Comp. Chem.* **1996**, *17*, 1571-1586.

(61) Schuchardt, K.L., Didier, B.T., Elsethagen, T., Sun, L., Gurumoorthi, V., Chase, J., Li, J., and Windus, T.L. *J. Chem. Inf. Model.* **2007**, *47*, 1045.

(62) Cizek, J. *Adv. Chem. Phys.* **1969**, *14*, 35-89.

(63) Purvis, G. D. I.; Bartlett, R. J. *J. Chem. Phys.* **1982**, *76*, 1910.

(64) Prinslow, D. A.; Armentrout, P. B. *J. Chem. Phys.* 1991, *94*, 3563.

(65)Chase, M.W., Jr.; Davies, C. A.; Downey, J.R., Jr.; Frurip, D. J.; McDonald, R. A.; Syverud, A. N. *J. Phys. Chem. Ref. Data* **1985**, *14*, Suppl. 1 (JANAF Tables).

UU IR Author Manuscript

(66) Moore, C. E. *Atomic Energy Levels, NSRDS-NBS 35* Washington, D. C., 1971; Vol. III.

(67) Yoshizawa, K.; Shiota, Y.; Yamabe, T. *J. Chem. Phys.* **1999**, *111*, 538-545.

(68) Gioumousis, G.; Stevenson, D. P. *J. Chem. Phys.* **1958,** *29*, 294.

(69) Miller, T. M.; Bederson, B. *Adv. Atomic Molec. Phys.* **1977**, *13*, 1.

(70) Rue, C.; Armentrout, P. B.; Kretzschmar, I.; Schröder, D.; Schwarz, H. *J. Chem. Phys.* **1999**, *110*, 7858.

(71) Herzberg, G. In *Molecular Spectra and Molecular Structure*, reprint edition; Krieger: Malabar, **1989**, Vol. I.

(72) Chesnavich, W. J.; Bass, L.; Su, T.; Bowers, M. T. *J. Chem. Phys.* **1981**, *74*, 2228.

(73) Angel, L. A.; Ervin, K. M. *J. Phys. Chem. A* **2006**, *110*, 10392.

(74) Jia, B.; Angel, L. A.; Ervin, K. M. *J. Phys. Chem. A.* **2008**, *112*, 1773.

(75) Boys, S. F.; Bernardi, R. *Molec. Phys.* **1970**, *19*, 553.

(76) van Duijneveldt, F. B.; van Duijneveldt de Rijdt, J. G. C. M.; van Lenthe, J. H. *Chem. Rev.* **1994**, *94*, 1873.

(77) Armentrout, P. B.; Chen, Y.-M. *J. Am. Soc. Mass Spectrom.* **1999**, *10*, 821-839.

(78) Li, R.; Balfour, W.J.; Hopkins, W. S.; Adam, A. G. *J. Molec. Spectros.* **2005**, *234*, 211-215.

UU IR Author Manuscript

TABLE 1: Bond Lengths, Vibrational Frequencies, and State Splittings for RuC^+ and RuS^+[a]

species	state	*r*, Å	ν, cm^{-1}	E_{rel}, [b] eV	
				B3LYP	CCSD(T)
RuC^+	$^2\Delta$	1.590, **1.503,** *1.593*	1156, **1723**	0.000	0.000
	$^4\Sigma^+$	1.669	967	1.488	1.448
	$^2\Sigma^+$	1.661	996	2.096	2.176
	$^4\Phi$	1.800	779	3.291	3.412
	$^6\Pi$	1.882	627	3.969	4.040
RuS^+	$^6\Sigma^+$	2.121, **2.089,** *2.107*	466, **457**	0.000	0.000
	$^4\Phi$	2.054	455	0.115	0.234
	$^4\Delta$	2.060	534	0.318	0.252
	$^2\Pi$	2.008	556	0.522	0.625
	$^2\Sigma^+$	1.986	610	0.803	1.003

[a] Geometry optimizations and frequency calculations performed at the B3LYP/Def2TZVPP (CCD/Def2TZVPP in bold and CCSD(T)/Def2TZVPP in italics) level of theory. [b] State splittings are single point energies calculated at the level of theory indicated using the Def2TZVPP basis set and the B3LYP/Def2TZVPP geometries including zero point energy corrections.

UU IR Author Manuscript

TABLE 2: Bond Lengths, Bond Angles, Vibrational Frequencies, and State Splittings for $RuCS^+$ [a]

species	state	*r*(Ru-C), Å	*r*(C-S), Å	∠RuCS, °	*ν*, cm^{-1}	E_{rel}, eV	
						B3LYP	CCSD(T)
CS	$^1\Sigma^+$		1.532		1311		
			1.527		**1362**		
			1.544				
$RuCS^+$	$^4\Sigma^+$	1.878	1.517	180.0	270 (2), 377, 1417	0.00	0.00
		1.922	**1.488**	**180.0**			
		1.877	*1.521*	*180.0*			
	$^2\Delta$	1.794	1.528	180.0	292 (2), 434, 1387	0.394	0.544
	$^6A''$	2.101	1.528	139.6	113, 342, 1214	2.536	2.409

[a] Geometry optimizations and frequency calculations performed at the B3LYP/Def2TZVPP (CCD/Def2TZVPP in bold, CCSD(T)/Def2TZVPP in italics) level of theory. [b] State splittings are single point energies calculated at the level of theory indicated using the Def2TZVPP basis set and the B3LYP/Def2TZVPP geometries including zero point energy corrections.

TABLE 3: Geometric Parameters, Vibrational Frequencies, and Relative Energies for Reactants, Products, Intermediates, and Transition States for Reaction of Ru^+ with CS_2[a]

species	state	*r*(Ru-S) Å	*r*(Ru-C) Å	*r*(C-S), Å *r*(S-S), Å	∠RuSC, ° ∠SRuC, ° ∠CSS, °	∠SCS, ° ∠RuCS, ° ∠RuSS, °	ν cm^{-1}	E_{rel}[b] eV
$Ru^+ + CS_2$	^4F			1.553 (2)[c]		180.0[d]	408 (2), 678, 1561	0.000 (0.000)
$Ru^+(SCS)$	$^4B_1$	2.554 (2)	2.020	1.594 (2)[c]	52.3 (2)[d]	178.2[d]	104, 200, 493, 533, 629, 1356	-1.932 (-1.902)
	$^2A_1$	2.440 (2)	1.966	1.595 (2)[c]	53.5 (2)[d]	171.7[d]	237, 245, 385, 476, 675, 1380	-1.473 (-1.441)
	$^2A_2$	2.408 (2)	1.923	1.598 (2)[c]	52.8 (2)[d]	171.5[d]	195, 237, 259, 487, 688, 1375	-1.244 (-1.258)
	$^2A_1$	2.518 (2)	1.992	1.596 (2)[c]	52.3 (2)[d]	176.8[d]	162, 201, 356, 525, 540, 1368	-1.205 (-1.178)
	$^2B_2$	2.670 (2)	2.141	1.580 (2)[c]	72.6[d]	179.1[d]	57, 157, 382, 422, 631, 1425	-0.348 (-0.551)
	$^6A'_a$	2.366 (2)	2.084	1.690 (2)[c]	59.1 (2)[d]	136.3[d]	212, 242, 316, 357, 668, 977	0.073 (0.007)
	$^6A'_b$	2.467	2.099	1.607[c] 1.684[c]	57.1[d]	133.4[d]	119, 213, 259, 333, 674, 1021	0.731 (0.162)
	$^4B_2$	2.989 (2)	1.983	1.647 (2)[c]	38.4 (2)[d]	139.0[d]	-79, 16, 177, 459, 763, 834	0.767 (0.559)
$SRuCS^+$ (TS)	$^4A''$	2.126	1.932	1.539,[c] 2.001[c]	55.7,[d] 58.9[e]	137.0,[d] 157.6[e]	-338, 195, 314, 391, 503, 1303	-1.304 (-1.311)
	$^2A''$	2.129	1.931	1.546,[c] 1.925[c]	56.6,[d] 56.4[e]	138.0,[d] 155.0[e]	-312, 184, 321, 396, 503, 1276	-0.632 (-0.839)
	$^2A'$	2.078	1.936	1.540,[c] 1.981[c]	56.9,[d] 59.0[e]	139.8,[d] 156.1[e]	-357, 193, 304, 388, 512, 1289	-0.571 (-0.643)
	^6A	2.228	2.111	1.543,[c] 2.127[c]	57.9,[d] 58.6[e]	117.9,[d] 178.7[e]	-407, 141, 158, 234, 380, 1221	0.636 (0.535)

UU IR Author Manuscript

	$^4A'$	2.327	1.995	1.557,[c] 2.011[c]	54.2,[d] 54.8[e]	125.4,[d] 163.6[e]	-379, 156, 261, 306, 350, 1174	1.070 (1.008)
$SRu^+(CS)$	$^4A''$	2.083	1.862	1.516[c]	95.1[e]	176.9[e]	102, 295, 345, 416, 503, 1406	-1.921 (-1.939)
	$^2A''$	2.090	1.848	1.518[c]	95.8[e]	177.7[e]	104, 298, 349, 422, 488, 1402	-1.642 *-1.555*
	$^2A'$	2.015	1.853	1.518[c]	97.5[e]	179.3[e]	106, 249, 302, 402, 559, 1397	-1.450 (-1.462)
	$^6\Sigma^+$	2.196	2.093	1.506[c]	180.0[e]	180.0[e]	69 (2), 252, 290 (2), 379, 1412	-0.934 (-0.769)
	$^6A'$ CP1	2.170	2.116	1.506[c]	156[e]	173[e]	-34, 190, 252, 268, 406, 1404	-0.792 (-0.649)
	$^4A''$ CP1	2.091	2.140	1.504[c]	163[e]	178[e]	-107, 84, 158, 257, 433, 1416	-0.641 (-0.646)
	$^4A'$	2.105	2.033	1.511[c]	126.4[e]	167.9[e]	45, 236, 240, 290, 408, 1370	-0.547 (-0.593)
	$^4\Phi$ ($^4A''$)	2.102	2.184	1.502[c]	180.0[e]	180.0[e]	-126, 27, 155, 234, 240, 417, 1429	-0.589 (-0.559)
	$^4\Delta$	2.122	2.100	1.509[c]	180.0[e]	180.0[e]	93(2), 239, 433, 1075 (2), 1390	-0.198 (-0.276)
	$^2\Delta$	2.028	2.189	1.504[c]	180.0[e]	180.0[e]	-161, -105, 151, 195, 229, 554, 1415	-0.208 (0.206)
	$^4A''$ CP2	2.056	3.262	1.509[c]	155[e]	178[e]	-82, -68, 24, 153, 457, 1390	0.412 (0.485)
TS_{SS}	$^4A''$	2.191	1.804	1.599[c] 2.463[f]	76.1[e]	129.5[e]	-336, 228, 304, 392, 652, 1009	-0.387 (-0.345)
	$^2A''$	2.136	1.878	1.584,[c] 2.748[f]	96.0[e]	104.8[e]	-200, -55, 205, 430, 556, 1011	-0.027 (0.280)
	$^2A'$	2.196	1.786	1.683[c] 2.208[f]	88.4[e]	104.1[e]	-193, 113, 261, 370, 659, 764	0.074 (0.093)

	^{6}A	2.262	1.890	1.692,[c] 2.239[f]	79.3[e]	105.0[e]	-373, 175, 268, 305, 608, 755	1.663 (1.677)
c-RuCSS$^+$	^{4}A″	2.280	1.780	1.674[c] 2.139[f]	77.7[e]	115.5[e]	212, 224, 309, 407, 721, 848	-0.590 (-0.502)
	^{2}A″	2.256	1.772	1.679[c] 2.146[f]	76.8[e]	117.3[e]	228, 254, 303, 405, 730, 842	-0.216 (-0.161)
	^{2}A′	2.307	1.738	1.742[c] 2.062[f]	77.4[e]	114.3[e]	208, 226, 229, 450, 674, 877	-0.017 (0.051)
	^{6}A	2.302	1.872	1.754[c] 2.098[f]	78.2[e]	105.3[e]	113, 221, 259, 427, 548, 727	1.615 (1.668)
	^{6}A″	2.331	1.862	1.774[c] 2.067[f]	77.6[e]	110.2[e]	-97, 182, 247, 477, 621, 741	1.703 (1.685)
TS_{CS}	^{2}A′	2.229	1.727	2.144[c] 1.967[f]	82.4[e] 79.5[g]	104.4[e] 93.8[g]	-352, 190, 277, 330, 581, 798	0.124 (0.368)
	^{4}A″	2.396	1.646	2.417[c] 1.968[f]	94.6[e] 86.2[g]	93.1[e] 86.2[g]	-269, 89, 208, 266, 598, 971	0.211 (0.250)
	^{2}A″	2.360	1.660	2.254[c] 1.975[f]	92.3[e] 87.8[g]	84.4[e] 95.5[g]	-370, -10, 214, 284, 585, 949	0.374 (0.418)
	^{6}A′	2.550	1.763	2.228[c] 2.017[f]	103.8[e] 107.7[g]	80.3[e] 68.2[g]	-355, 130, 137, 227, 555, 770	1.953 (2.115)
CRu$^+$(SS)	^{4}A′	2.455 (2)	1.614	1.978[f]	112.6 (2)[e]	66.3 (2)[g]	134, 183, 225, 239, 615, 1101	-0.367 (-0.307)
	^{2}A′	2.214	1.618	1.882[f]	100.3[e]	121.4[g]	118, 127, 270, 308, 701, 1079	-0.013 (-0.099)
	^{4}A″	2.467	1.602	1.928[f]	113.2[e]	104.9[g]	-14, 78, 149, 232, 649, 1131	0.012 (0.036)
	^{2}A″$_a$	2.337	1.603	1.906[f]	105.9[e]	120.0[g]	-37, 100, 219, 245, 671, 1127	0.122 (-0.003)
	^{2}A	2.268	1.614	1.891[f]	101.6[e]	119.4[g]	96, 120, 214, 264, 696, 1091	0.148 (0.123)
	^{2}A″$_b$	2.468	1.603	1.929[f]	113.1[e]	104.5[g]	14, 78, 151, 231, 644, 1128	0.294 (0.243)

	$^6A'$	2.492	1.697	1.957[f]	128.7[e]	61.9[e]	78, 101, 149,	1.700
					89.5[g]	79.9[g]	216, 641, 913	(1.803)
TS_{RuS}	$^4A''$	3.301	1.712	1.706[c]	53.6[e]	143.7[e]	-117, 216, 273,	0.466
				1.995[f]	91.9[g]	70.8[g]	499, 563, 978	(0.283)
	$^2A'$	3.165	1.706	1.725[c]	56.6[e]	140.1[e]	-119, 193, 262,	0.570
				2.006[f]	89.9[g]	73.3[g]	496, 568, 1006	(0.405)
	$^2A''$	3.245	1.691	1.706[c]	54.4[e]	143.5[e]	-119, 224, 272,	0.715
				2.005[f]	90.6[g]	71.5[g]	491, 565, 1058	(0.624)
	^6A	2.539	1.830	1.775[c]	72.7[e]	112.9[e]	-695, 126, 129,	1.725
				2.024[f]	88.3[g]	81.5[g]	508, 603, 657	(1.710)
$RuCSS^+$	$^4A''$		1.708	1.689[c]	102.4[g]	179.8[e]	72, 228, 316,	0.340
				1.978[f]			422, 534, 1029	(0.115)
	$^2A'$		1.700	1.695[c]	99.7[g]	179.2[e]	74, 242, 314,	0.427
				1.995[f]			417, 517, 1072	(0.202)
	$^2A''$		1.684	1.697[c]	103.1[g]	179.3[e]	76, 235, 322,	0.570
				1.980[f]			432, 528, 1071	(0.418)
	$^6A'$		1.851	1.616[c]	110.0[g]	166.0[e]	55, 253, 309,	1.324
				2.041[f]			378, 384, 1090	(1.140)
RuS^+	$^6\Sigma^+$ +	2.121					466	1.169
+ CS	$^1\Sigma^+$			1.532[c]			+ 1311	(1.377)
$RuCS^+$	$^4\Sigma^-$ +		1.878	1.517[c]		180.0[e]	270 (2), 377,	1.293
+ S	^3P						1417	(1.425)
RuC^+	$^2\Delta$ +		1.590				1156	1.260
+ S_2	$^3\Sigma^-$			1.904[f]			+ 715	(1.290)

[a] All geometrical parameters are calculated at the B3LYP/Def2TZVPP level of theory. [b] Relative energies calculated at CCSD(T)/Def2TZVPP//B3LYP/Def2TZVPP (B3LYP/Def2TZVPP) levels of theory, corrected for zero point energies. Absolute calculated energies for the ground state $Ru^+ + CS_2$ asymptote are 927.832727 (929.112010) E_h, including zero point energies. [c] r(C-S). [d] ∠RuSC and ∠SCS. [e] ∠SRuC and ∠RuCS. [f] r(S-S). [g] ∠CSS and ∠RuSS.

UU IR Author Manuscript

TABLE 4: Summary of Parameters in Eqs 4 and 5 Used to Analyze the Cross Sections for Reactions 1 – 3[a]

Reaction	σ_0	n	E_0, eV[a]	$D_0(Ru^+\text{-}X)$, eV
$Ru^+ + CS_2 \rightarrow RuC^+ + S_2$	1.0 (0.2)[b]	0.8 (0.3)	1.33 (0.16)	6.17 (0.18)
	1.1 (0.4)[c]	0.5 (0.2)	1.20 (0.06)	6.30 (0.10)
	1.6 (1.3)[d]	0.7 (0.3)	1.26 (0.15)	6.24 (0.17)
$\rightarrow RuS^+ + CS$	3.2 (0.6)[b]	1.1 (0.2)	1.51 (0.04)	2.99 (0.06)
	2.8 (0.8)[c]	0.5 (0.2)	1.47 (0.06)	3.03 (0.10)
	2.3 (0.6)[d]	0.7 (0.3)	1.44 (0.06)	3.06 (0.10)
$\rightarrow RuCS^+ + S$	0.40 (0.14)[b]	2.0 (0.5)	1.88 (0.16)	2.62 (0.16)
	29 (16)[c]	0.5 (0.2)	1.92 (0.16)	2.58 (0.18)
	24 (14)[d]	0.7 (0.3)	1.91 (0.16)	2.59 (0.18)

[a] Uncertainties in parentheses with values for E_0 being two standard deviations. [b] Single channel fit using eq 4 and $m = 1$. [c] Competitive fit using eq 5 and loose (PSL) transition states for all three product channels. [d] Competitive fit using eq 5 with transition state switching for reaction 1.

UU IR Author Manuscript

TABLE 5: Experimental and Theoretical Bond Energies (eV)[a]

bond	exp	B3LYP	CCSD(T)//B3LYP	CCSD(T)//CCD	CCSD(T)
Ru^+—S	3.04 ± 0.10	3.127 (3.323)	2.933 (3.186)	2.927 (3.185)	2.962 (3.217)
Ru^+—CS	2.59 ± 0.18	3.085 (3.275)	2.935 (3.062)	2.902 (3.022)	2.854 (3.122)
Ru^+—C	6.27 ± 0.15	5.934 (6.122)	5.938 (6.066)	5.638 (5.786)	6.000 (6.138)
	4.70 ± 0.11[b]				
	6.16 ± 0.07[c]				
MAD[d]		0.27 ± 0.21	0.22 ± 0.12	0.32 ± 0.20	0.17 ± 0.09

[a] In all cases, theoretical values are obtained at the level shown using the Def2TZVPP basis set. Values are corrected for zero point energies and basis set superposition errors at the full counterpoise limit. Values without counterpoise corrections are in parentheses.

[b] Reference 77.

[c] Average value, derived as discussed in the text.

[d] Mean absolute deviation from experimental values.

UU IR Author Manuscript

Figure Captions

Figure 1. Reaction coordinate diagram for reaction of Ru^+ in quartet (blue line) , sextet (red line), and doublet (light green – A′, dark green – A″) states with CS_2. All energies are calculated at the CCSD(T)//B3LYP level including zero point energies. Part a) shows the surfaces for association of Ru^+ and CS_2 and insertion of Ru^+ into the CS bond, where both bent and linear $SRu^+(CS)$ intermediates are indicated. Part b) shows dissociation of the $SRu^+(CS)$ intermediates into the products of reactions 1 – 3. Large dots indicate crossing points between the quartet and sextet surfaces.

Figure 2. Quartet spin intermediates, transition states, and products calculated at the B3LYP/Def2TZVPP level of theory in the order of the reaction coordinate diagram of Figure 1. Bond lengths are shown in Å. All species are planar except for $CRu^+(SS)$. Atoms are color coded as ruthenium – blue, carbon – grey, and sulfur – yellow.

Figure 3. Doublet spin intermediates, transition states, and products calculated at the B3LYP/Def2TZVPP level of theory in the order of the reaction coordinate diagram of Figure 1. Bond lengths are shown in Å. All species are planar. Atoms are color coded as ruthenium – blue, carbon – grey, and sulfur – yellow.

Figure 4. Sextet spin intermediates, transition states, and products calculated at the B3LYP/Def2TZVPP level of theory in the order of the reaction coordinate diagram of Figure 1. Bond lengths are shown in Å. Nonplanar species have the ∠SRuCS dihedral angle indicated. Atoms are color coded as ruthenium – blue, carbon – grey, and sulfur – yellow.

UU IR Author Manuscript

Figure 5. Relaxed potential energy surface scans at the B3LYP/Def2TZVPP level of theory for bending the $SRu^+(CS)$ intermediate (parts a and b) and for stretching the SRu^+-CS bond (part c). Results are shown for optimization along the quartet (parts a and c) and sextet (part b) surfaces with single point energies at the same geometries for the other spin state. Approximate crossing points (CP) between the surfaces are indicated by dots with geometries shown in parts d - f.

Figure 6. Product cross sections for the reaction of Ru^+ with CS_2 to form RuC^+ (circles), RuS^+ (squares), and $RuCS^+$ (inverted triangles) as function of center-of-mass energy (lower axis) and laboratory energy (upper axis). Results are shown for Ru^+ formed without (closed symbols) and with (open symbols) methane quenching gas in the flow tube. The LGS collision cross section (scaled by a factor of 500) is shown by the line.

Figure 7. Cross sections for the reaction of ground state Ru^+ (^4F) with CS_2 to form RuC^+ (closed circles), RuS^+ (open squares), and $RuCS^+$ (closed inverted triangles) as function of center-of-mass energy (lower axis) and laboratory energy (upper axis). The line shows the total cross sections and the arrow marks D_0(S-CS) = 4.50 eV.

Figure 8. Cross sections for the reaction of ground state Ru^+ (^4F) with CS_2 to form RuC^+ (closed circles), RuS^+ (open squares), and $RuCS^+$ (closed inverted triangles) as function of center-of-mass energy (lower axis) and laboratory energy (upper axis). Solid lines show the competitive model cross sections given by eq 5 and the parameters given in Table 4 for the model using transition state switching for reaction 1. Dashed lines show these models in the absence of experimental kinetic energy distributions for reactants at 0 K.

UU IR Author Manuscript

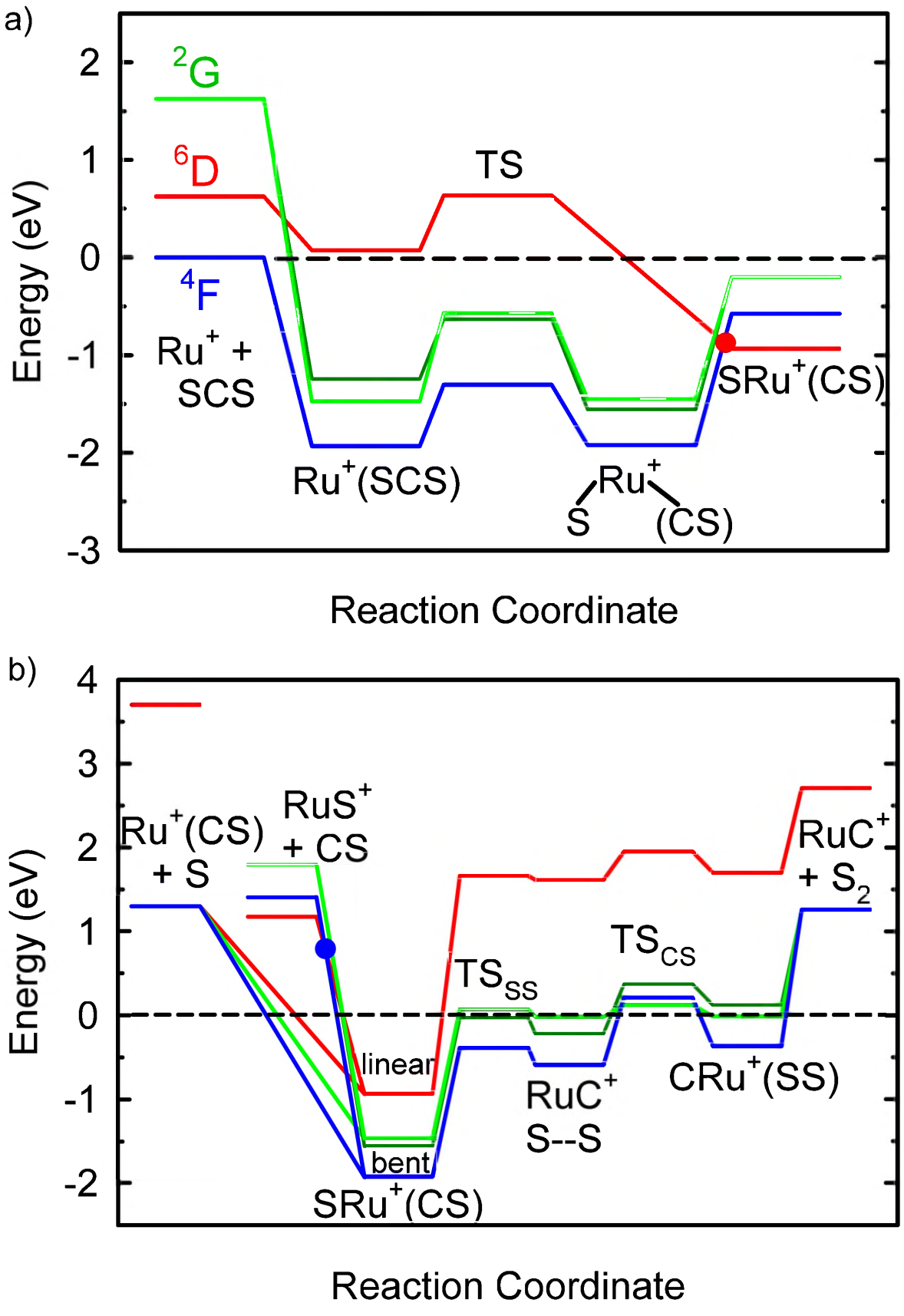

Figure 1

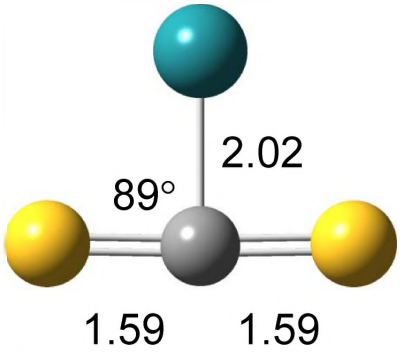

$Ru^{+}(SCS)\ ^{4}B_{1}$

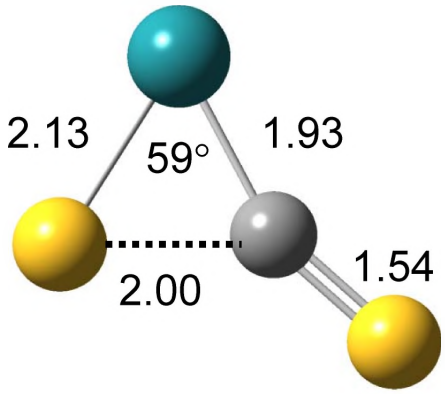

TS $^{4}A''$

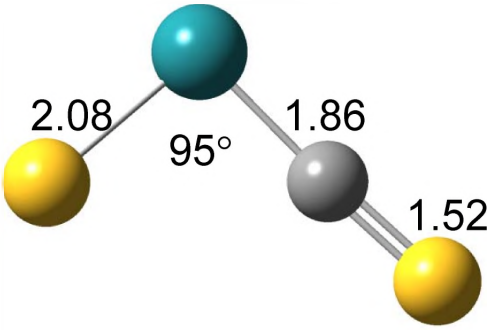

$SRu^{+}(CS)\ ^{4}A''$

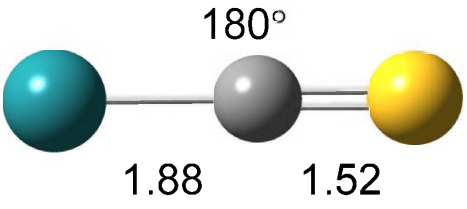

$Ru^{+}(CS)\ ^{4}\Sigma^{+}$

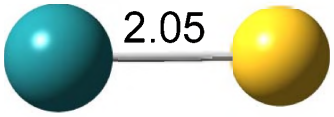

$RuS^{+}\ ^{4}\Phi$

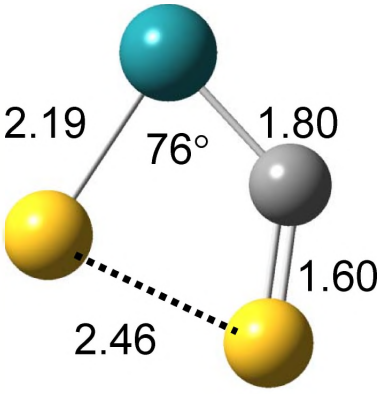

$TS_{SS}\ ^{4}A''$

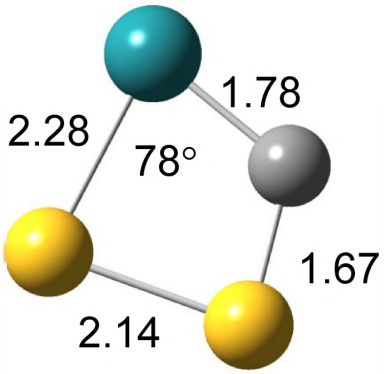

c-RuCSS $^{4}A''$

Figure 2

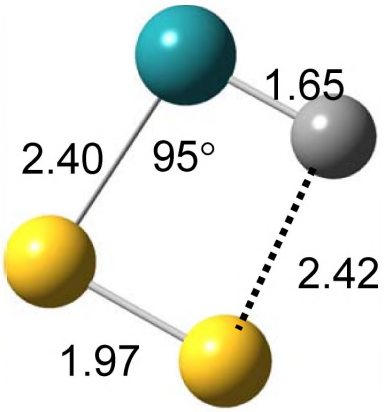

TS_{CS} $^4A''$

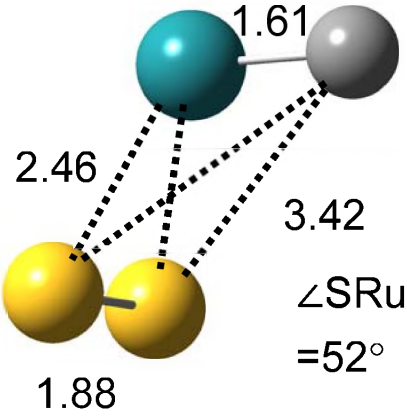

$CRu^+(SS)$ $^4A'$

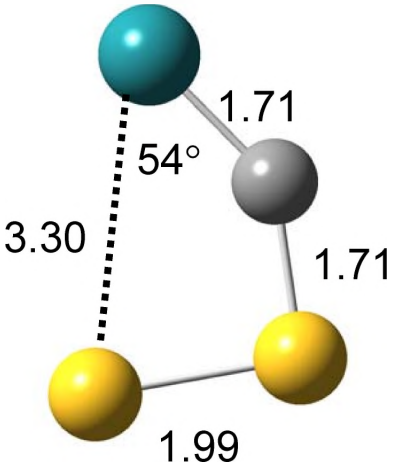

TS_{RuS} $^4A''$

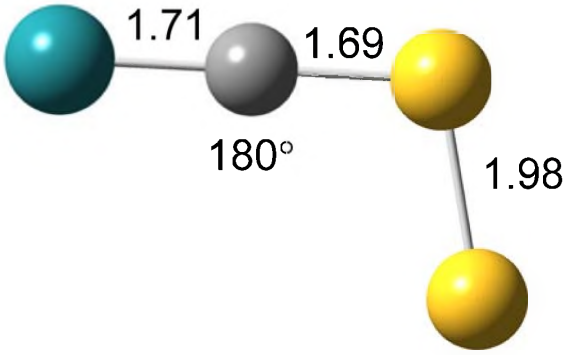

$RuCSS^+$ $^4A''$

Figure 2

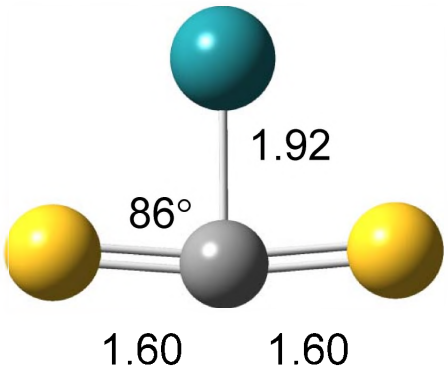

$Ru^{+}(SCS)\ ^{2}A_{2}$

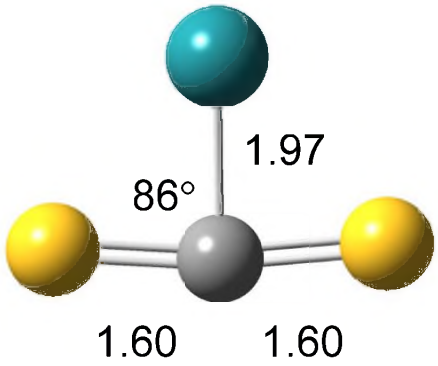

$Ru^{+}(SCS)\ ^{2}A_{1}$

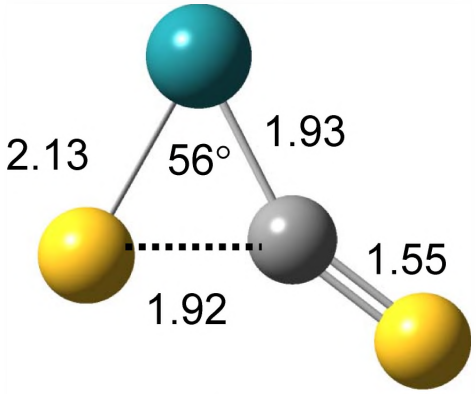

TS $^{2}A''$

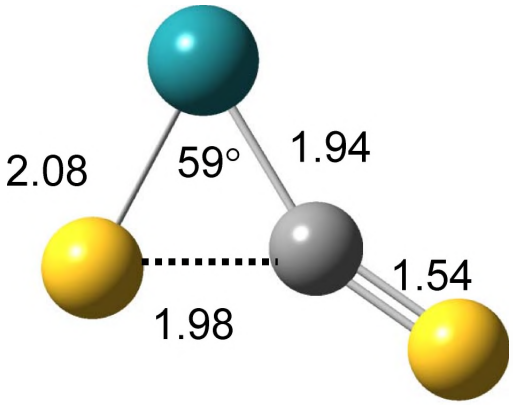

TS $^{2}A'$

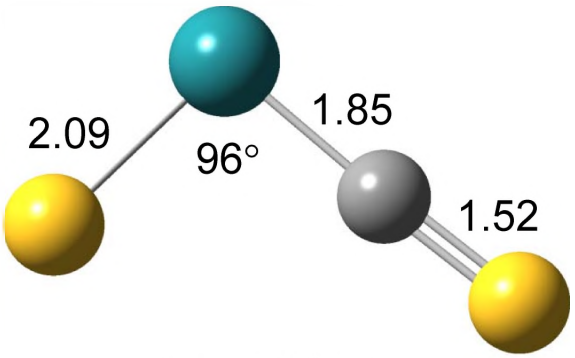

$SRuCS^{+}\ ^{2}A''$

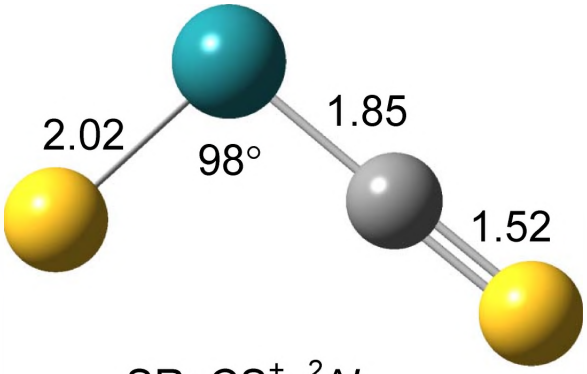

$SRuCS^{+}\ ^{2}A'$

$RuS^{+}\ ^{2}\Pi$

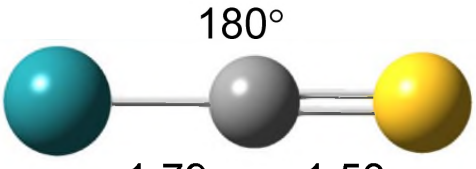

$Ru^{+}(CS)\ ^{2}\Delta$

Figure 3

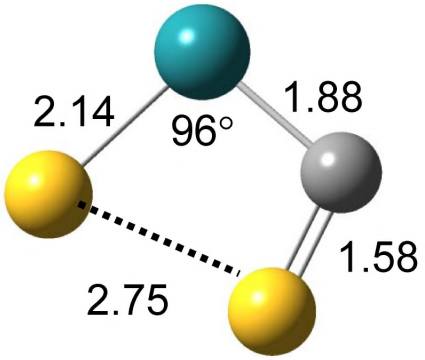

TS_{SS} $^2A''$

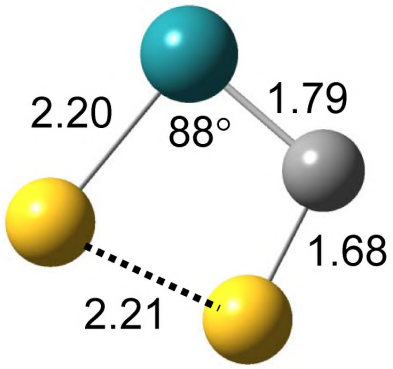

TS_{SS} $^2A'$

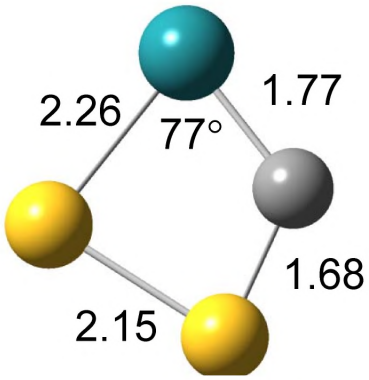

c-RuCSS $^2A''$

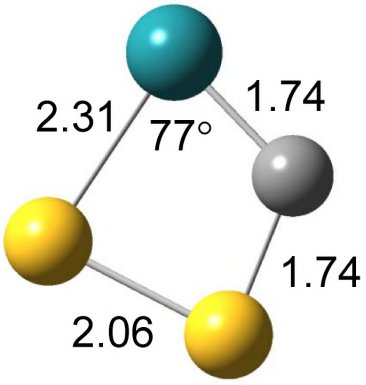

c-RuCSS $^2A'$

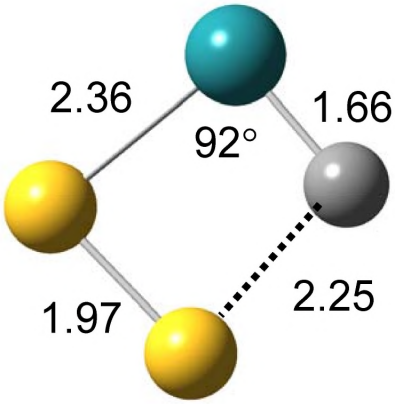

TS_{CS} $^2A''$

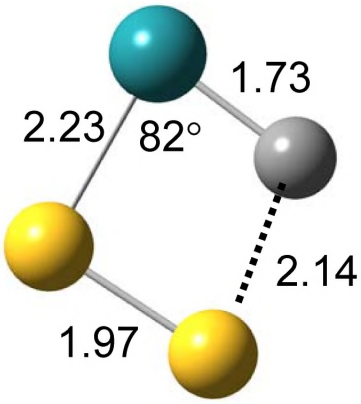

TS_{CS} $^2A'$

Figure 3

UU IR Author Manuscript

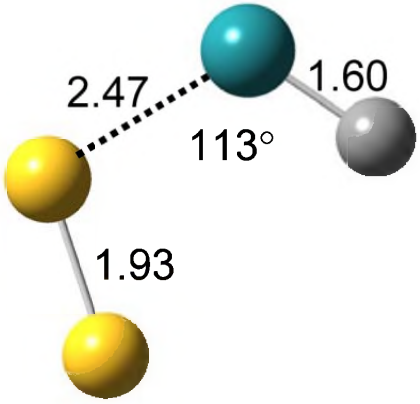

$CRu^{+}(SS)\ {}^{2}A''$

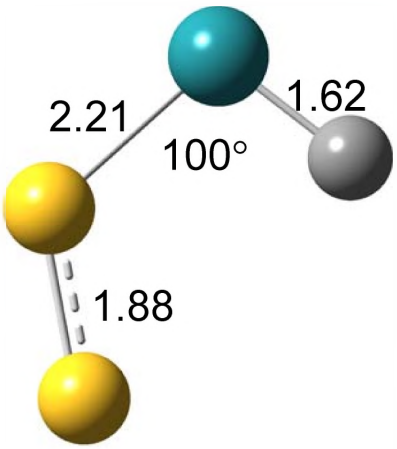

$CRu^{+}(SS)\ {}^{2}A'$

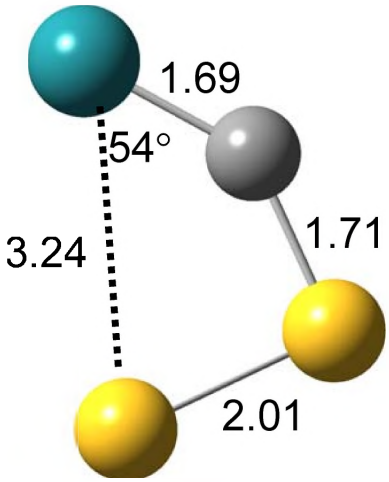

$TS_{RuS}\ {}^{2}A''$

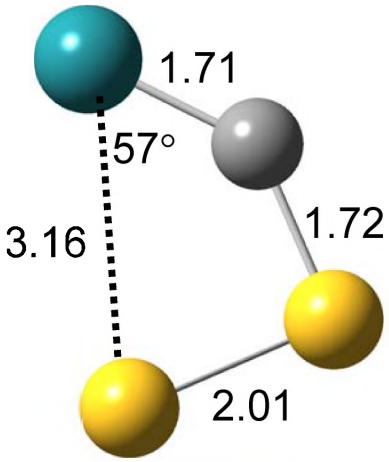

$TS_{RuS}\ {}^{2}A'$

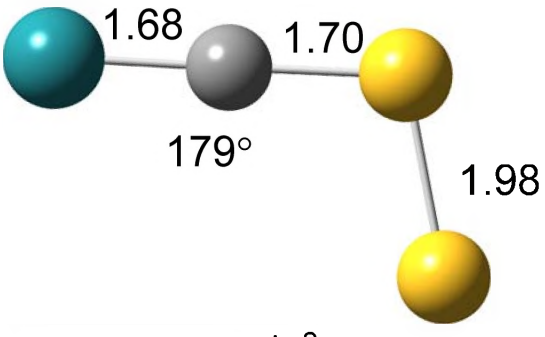

$RuCSS^{+}\ {}^{2}A''$

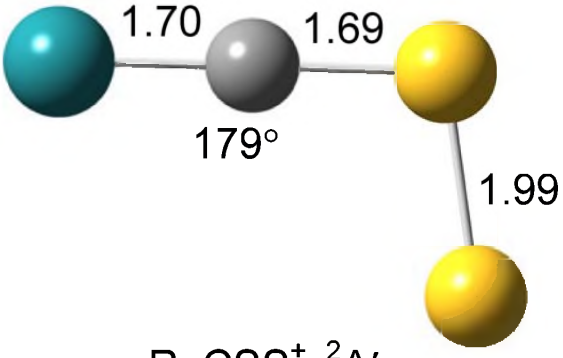

$RuCSS^{+}\ {}^{2}A'$

Figure 3

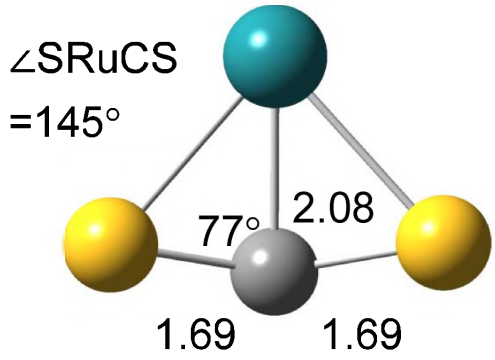

$Ru^{+}(SCS)\ {}^{6}A'_{a}$

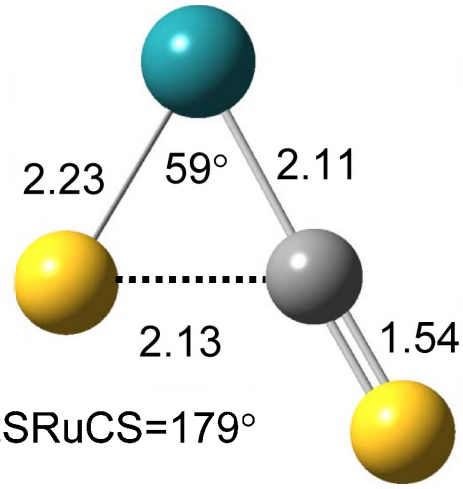

TS ^{6}A

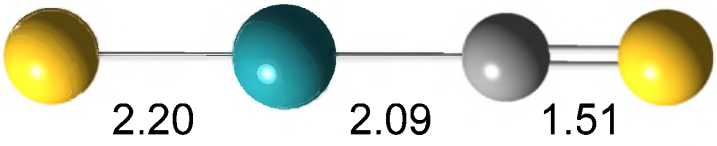

$SRuCS^{+}\ {}^{6}\Sigma^{+}$

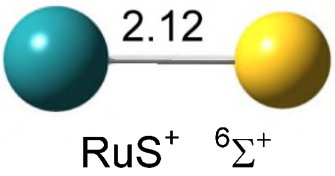

$RuS^{+}\ {}^{6}\Sigma^{+}$

$Ru^{+}(CS)\ {}^{6}A''$

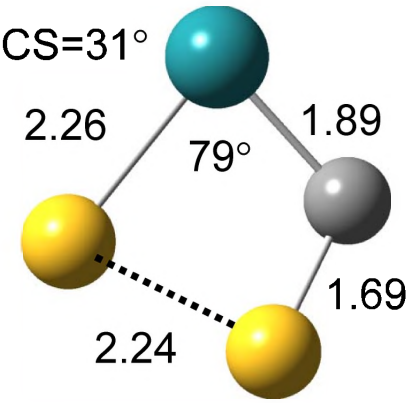

$TS_{SS}\ {}^{6}A$

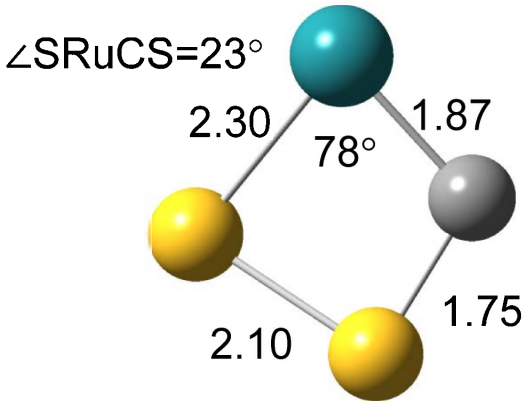

c-RuCSS ^{6}A

Figure 4

UU IR Author Manuscript

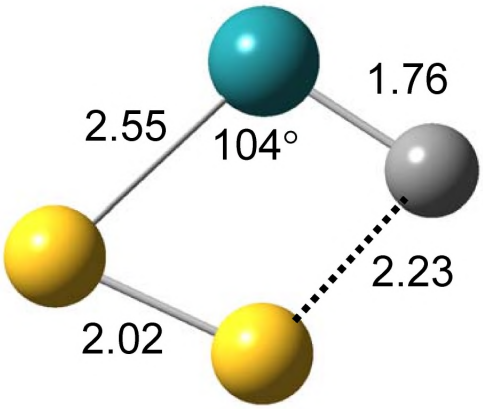

TS_{CS} $^6A'$

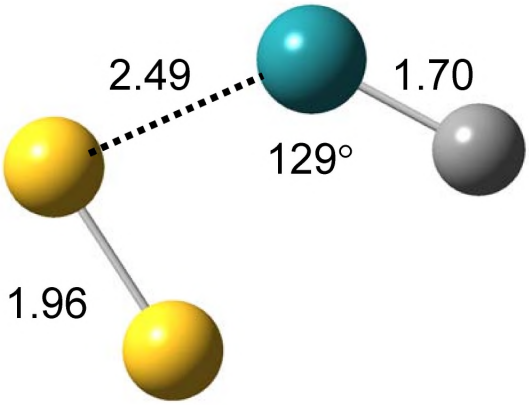

$CRu^+(SS)$ $^6A'$

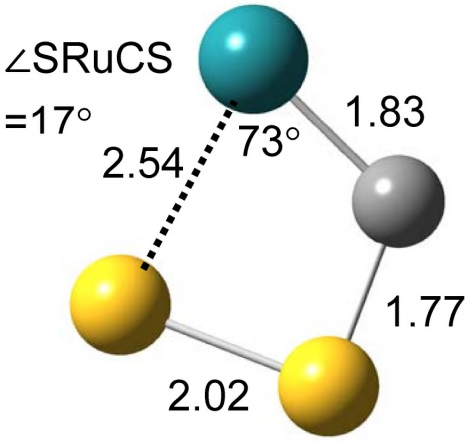

TS_{RuS} ^6A

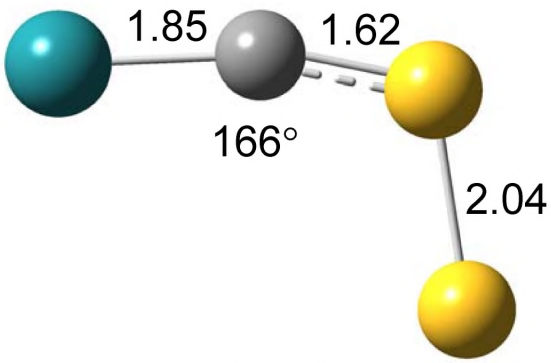

$RuCSS^+$ $^6A'$

Figure 4

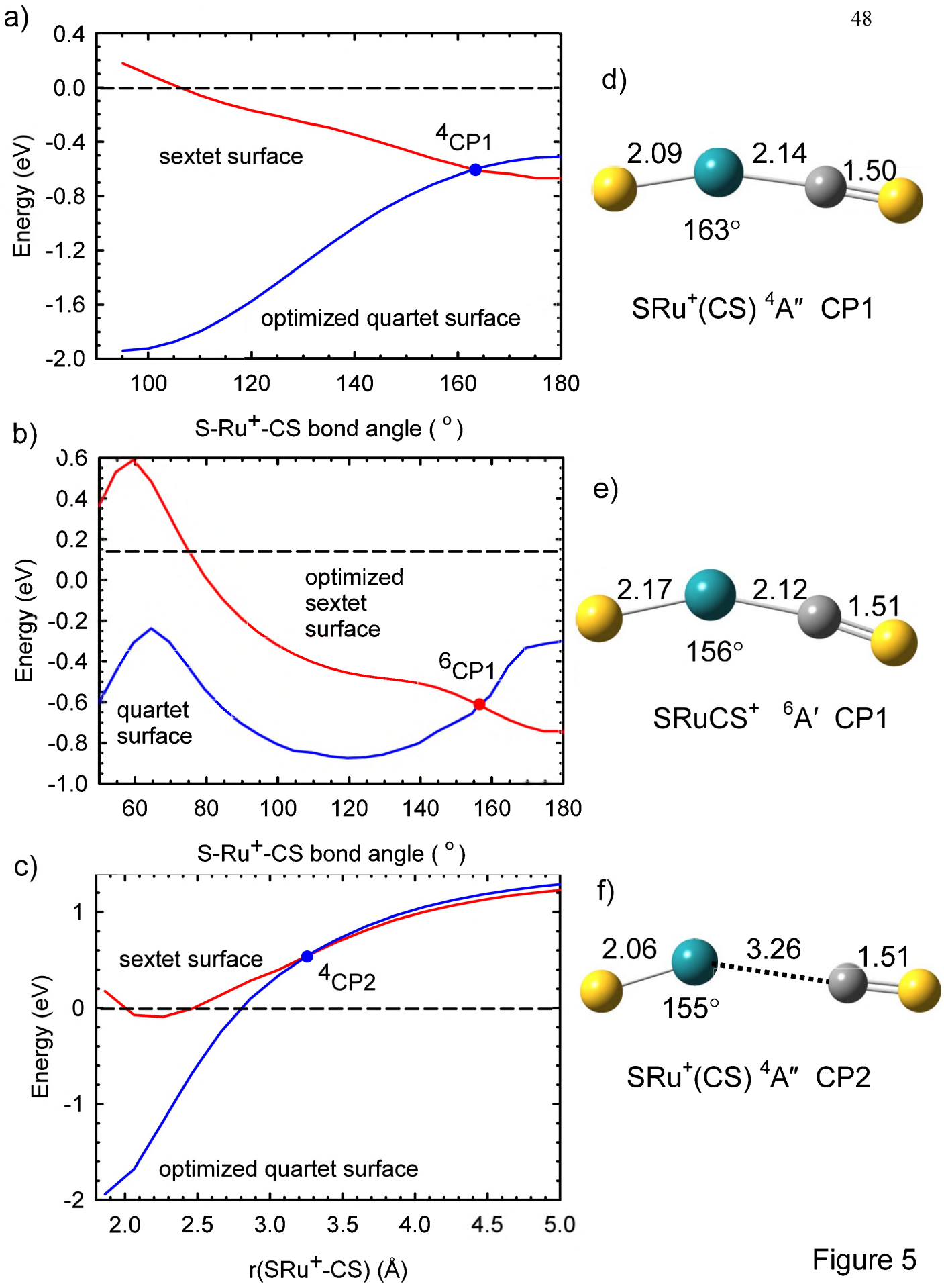

Figure 5

UU IR Author Manuscript

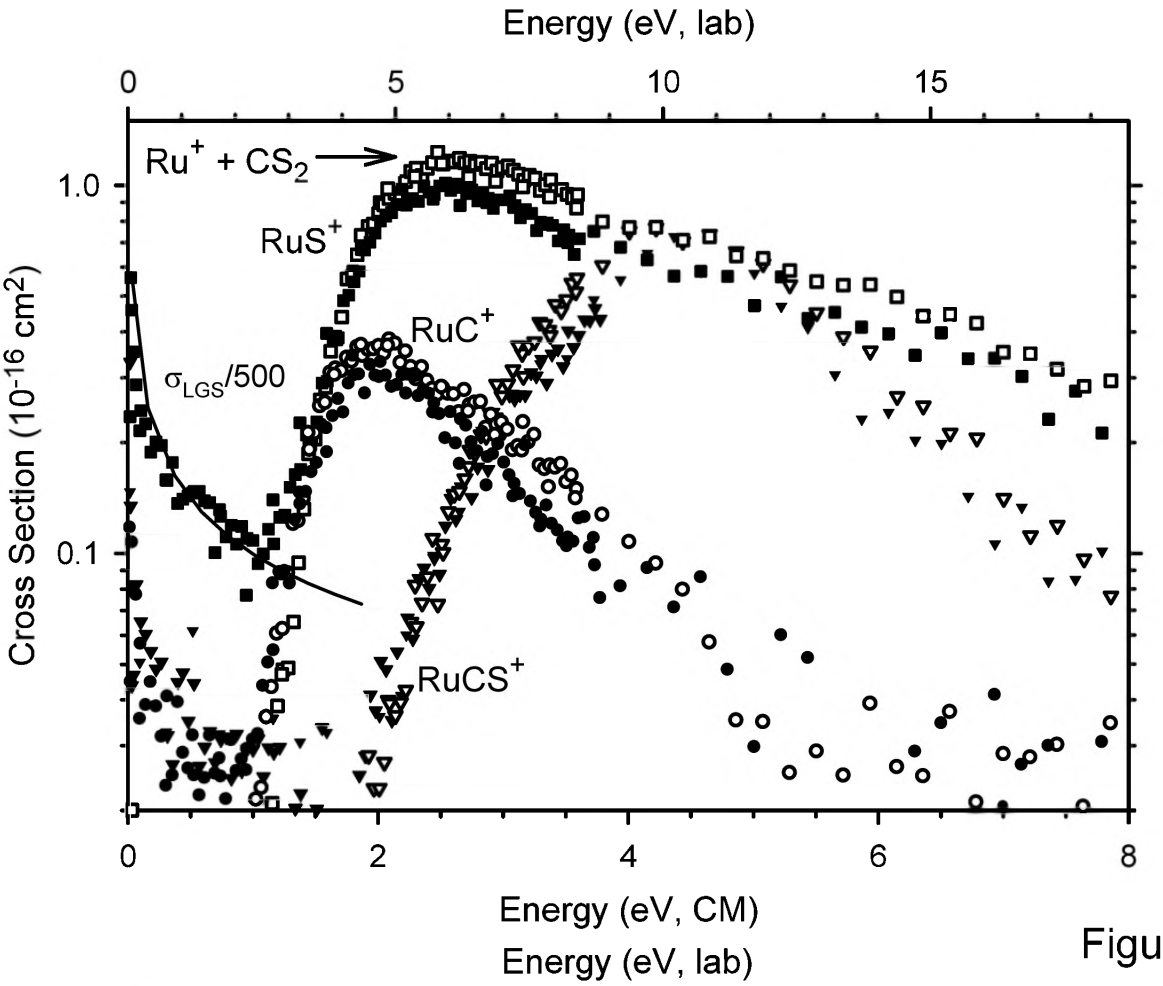

Figure 6

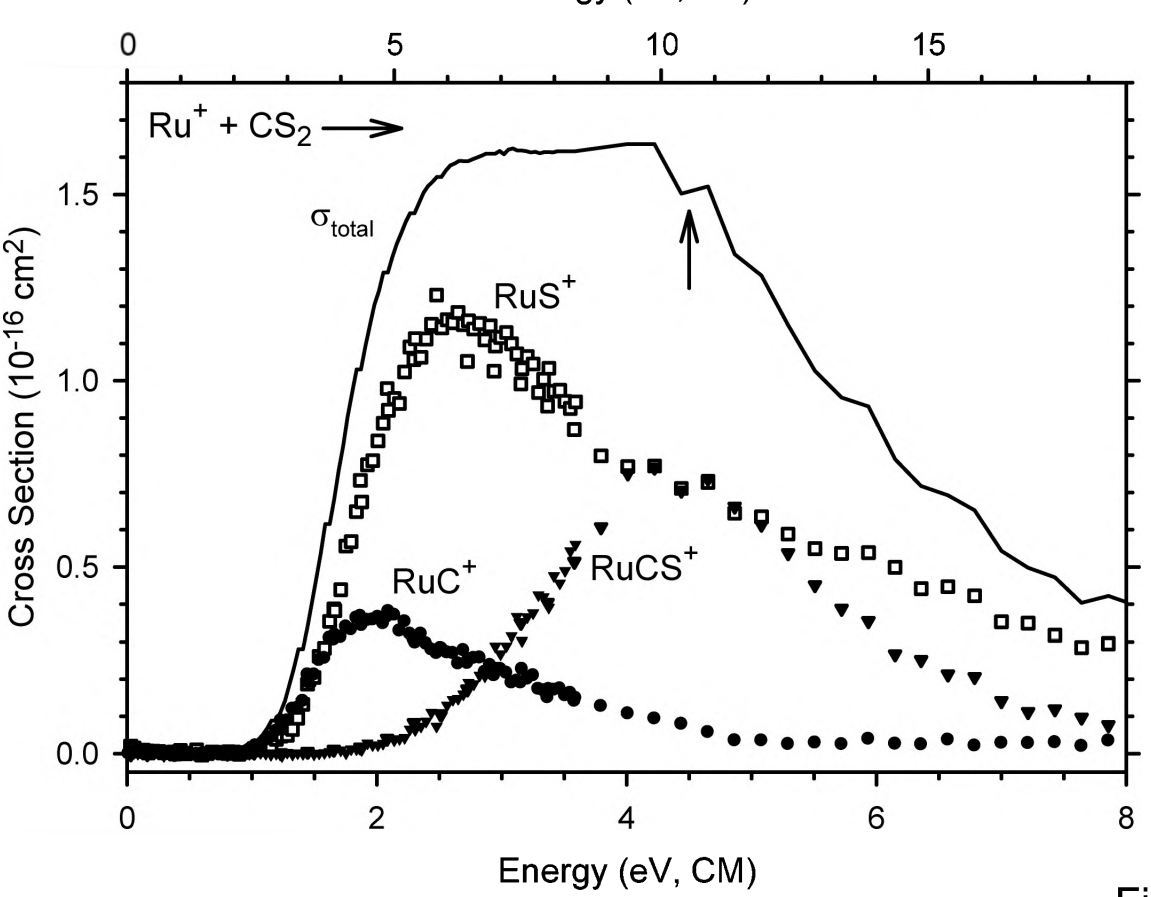

Figure 7

UU IR Author Manuscript

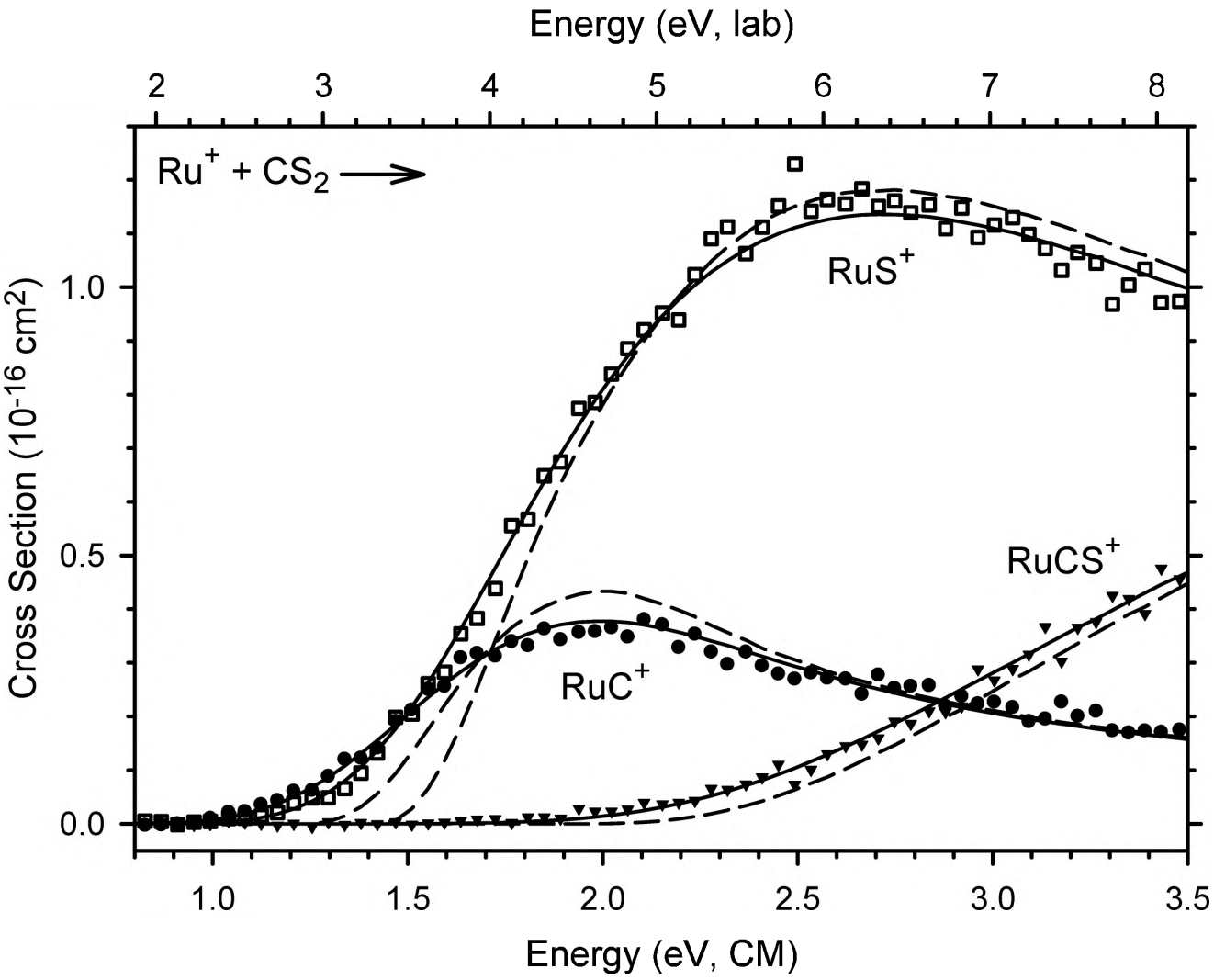

Figure 8

UU IR Author Manuscript